A DIFFERENTIAL ABSORPTION TECHNIQUE FOR THE DETECTION OF NITROGEN DIOXIDE AS AN ATMOSPHERIC POLLUTANT

A THESIS

Presented to

The Faculty of the Division of Graduate

Studies and Research

By

Lee G. Dodge

In Partial Fulfillment

of the Requirements for the Degree

Master of Science in Physics

Georgia Institute of Technology

January, 1973

A DIFFERENTIAL ABSORPTION TECHNIQUE FOR THE DETECTION OF NITROGEN DIOXIDE AS AN ATMOSPHERIC POLLUTANT

Approved:

D. C. O'Shea, Chairman

T. L. Weatherly

M. J. Matteson

Date approved by Chairman: 1/22/73

ACKNOWLEDGMENTS

The author would like to express his thanks to Dr. D. C. O'Shea for his guidance and many helpful suggestions throughout this research effort. The contributions of the reading committee, including Dr. T. L. Weatherly and Dr. M. J. Matteson, are appreciated. The members of the Special Techniques Branch of the Georgia Tech Engineering Experiment Station, in particular Mr. J. J. Gallagher, Mr. A. McSweeny, Mr. J. B. Langley II, and Mr. R. G. Shackelford, are thanked for their suggestions and the use of their White cell. The use of equipment loaned by Dr. J. Q. Williams and Dr. R. E. Little is appreciated, as is the help given by Mr. V. P. Mallette. Financial assistance for this project was provided by the Environmental Protection Agency and the School of Physics at the Georgia Institute of Technology.

Ms. Mary Ann Owen is thanked for typing the manuscript and Miss Lindsay Shepherd for helping to proofread it.

TABLE OF CONTENTS

TABLE OF CONTENTS (Continued)

LIST OF TABLES

LIST OF ILLUSTRATIONS

NOMENCLATURE

A	amperes
C	centigrade
$C^{o}_{N_2O_4}$	ideal concentration of N_2O_4 for no dissociation
C_N	measure of turbulence
D	diameter
E	energy
E_e	electronic energy
E_f	final energy
E_i	initial energy
E_r	rotational energy
E_t	translational energy
E_v	vibrational energy
EPA	Environmental Protection Agency
I	light intensity
I^{o}	light intensity without attenuation effects
I^{R}	light intensity at distance R
$\bar{I}$	mean light intensity
$K_{N_2O_4}$	dissociation constant
N	chemical symbol for nitrogen
O	chemical symbol for oxygen
P	measured pressure
P_{wc}	pressure in White cell

NOMENCLATURE (Continued)

R	total path length
R	gas constant
T	temperature
V	volume
V	visibility
V_a	measurement volume in NO_2 feed system
V_{wc}	volume of White cell
atm	*atmosphere (pressure)*
c	concentration
c	speed of light
cm	centimeters
f	focal length of lens
h	Planck's constant
$\hbar$	Planck's constant divided by 2π
k	Boltzmann's constant
k	kilo-(prefix)
k	wavenumber
l	liter
m	meter
m	mass of atom or molecule
m	milli-(prefix)
mmHg	millimeters of mercury (pressure)
n	density of molecules
n	nano-(prefix)

NOMENCLATURE (Continued)

p	partial pressure
ppm	parts per million
$p^{o}_{N_2O_4}$	ideal pressure of N_2O_4 for no dissociation
r	path length
rpm	rotations per minute
t	time
$\bar{v}$	mean molecular velocity
y	constant in concentration equation
Δ	prefix for spread or uncertainty in quantity
θ	divergence angle
α	degree of dissociation
α	non-wavelength dependent refractive index scattering coefficient
$\alpha(\lambda)$	absorption coefficient at wavelength λ
$\bar{\alpha}_{\lambda}$	measured absorption coefficient for wavelength λ
β	Rayleigh scattering coefficient
γ	refractive index fluctuation scattering coefficient
δ	Mie scattering coefficient
λ	wavelength
μ	micro-(prefix)
ν	frequency
σ	absorption coefficient
σ_o	scattering cross-section
τ	mean collision time

SUMMARY

The theory for a laser technique for the detection of nitrogen dioxide (NO_2) as an atmospheric pollutant is developed and experimental results are given. The measurement scheme is based on the difference in absorption by nitrogen dioxide of two wavelengths of an argon-ion laser as it propagates through the atmosphere. Although tests in the atmosphere are not complete, preliminary results indicate that ambient urban NO_2 concentrations (.01-.20 ppm) can probably be detected and measured by a light absorption technique over a path length of seven km.

The production and properties of nitrogen dioxide as an atmospheric pollutant are discussed, along with the methods which have been used or suggested for its measurement. The most feasible methods of remote optical sensing of pollutants in the atmosphere are presented and the reasons for selecting the absorption technique are discussed.

The mathematical absorption theory is developed and includes attenuation parameters for scattering processes in addition to the absorption by NO_2. Possible interferences by other light absorbing gases are considered.

The absorption spectrum of NO_2 in the visible region is presented and the absorption coefficients for the discrete output wavelengths of a mercury lamp and an argon-ion laser are given. An

experiment is described which was designed to use these absorption coefficients of NO_2 for the argon-ion laser to measure the NO_2 concentration in the atmosphere on a real time basis.

CHAPTER I

INTRODUCTION

Nitrogen Dioxide as an Air Pollutant

Production of NO_2 and Atmospheric Reactions

Of the various oxides of nitrogen, the most important as air pollutants are nitric oxide (NO) and nitrogen dioxide (NO_2),[1] which are jointly labeled as NO_X. They are interconverted in the atmosphere with their ratio depending on conditions such as the amount of sunlight, hydrocarbons, and ozone present. NO_X is emitted into the atmosphere in three different concentration ranges:

(1) localized as NO_2 and NO in high concentration but small total amounts from nitric acid or nitration processes;

(2) somewhat localized as NO (initially) in intermediate concentration but large total amounts from combustion processes;

(3) non-localized as NO_X in the ambient atmosphere in low concentrations but very large total amounts from the biological nitrogen cycle.

The natural nitrogen cycle introduces NO_X into the atmosphere at a concentration of several parts per billion, and when removed from the air by rain and converted to nitrates, it serves as a vital fertilizer for plants. The normal urban concentration of 0.02 to 0.2 parts per million (ppm) is considerably higher than the natural concentration and is due principally to internal combustion engines (one-half of

man-made amount), electrical power plants (one-third), and heating requirements and industrial processes. The NO_x emission concentration from stationary combustion sources is typically 50 to 1000 ppm, and from nitric acid plants is 1000 to 10,000 ppm.[2]

Almost all of the NO_x initially formed during combustion is NO, which is subsequently oxidized in the atmosphere to the more toxic and irritating NO_2. During high temperature combustion processes, NO is formed in an endothermic reaction:

$$N_2 + O_2 \rightleftarrows 2NO. \qquad (1)$$

The NO is emitted into the atmosphere and is probably partially converted to NO_2 by a series of reactions

$$NO + O_2 \rightleftarrows NO_3 \qquad (2)$$

$$NO_3 + NO \rightarrow 2NO_2. \qquad (3)$$

The conversion to NO_2 by this process is appreciable only when the NO concentration is greater than 100 ppm. Most of the NO_2 formation is due to more complicated reactions involving absorption of sunlight and interaction with hydrocarbons, oxygen, and ozone. While these reactions are complex and varied,[3] they are important in the field of air pollution because the resulting photochemical oxidants are very destructive to plant and animal (including human) life.[1] One particular-

ly important photochemical reaction involving NO_2 and leading to photochemical oxidants is

$$NO_2 \xrightarrow{\text{sunlight}} NO + O.$$

Detrimental Effects of Nitrogen Oxides

Although NO_X is most harmful as a pollutant in its interactions leading to photochemical smog, NO and particularly NO_2 in themselves cause material damage and adverse health effects. Nitrogen dioxide reaction products have been shown to cause corrosion and failure of electrical components where average NO_X levels were 0.066 to 0.084 ppm (124 to 158 $\mu g/m^3$).[1]

Adverse health effects in the form of greater incidence of acute bronchitus among infants and school children have been observed when the mean 24 hour NO_2 concentration varied from 0.063 to 0.083 ppm (118 to 156 $\mu g/m^3$).[1] Increased incidence of acute respiratory disease has been observed in family groups when the mean NO_2 concentration was 0.062 to 0.109 ppm (117 to 205 $\mu g/m^3$),[1] as measured by the Jacobs-Hochheiser method.[4] These studies were used in setting the national primary and secondary ambient air quality standard for nitrogen dioxide, which is 0.05 ppm (100 $\mu g/m^3$) - annual arithmetic mean as measured by the Jacobs-Hochheiser technique.[4]

Measurement Techniques for Nitrogen Dioxide

It has recently been reported that the efficiency factors associated with the Jacobs-Hochheiser reference method are in considerable error, and the resulting calculated values of NO_2 concen-

tration are too high.[5,6] The Jacobs-Hochheiser method can be described briefly as a chemical technique whereby NO_2 is collected by bubbling air through a sodium hydroxide solution to form a stable solution of sodium nitrite. The nitrite ion produced during sampling is determined colorimetrically by reacting the exposed absorbing reagent with phosphoric acid, sulfanilamide, and N-1-napthyl-ethylenediamine dihydrochloride. The samples are usually taken over a 24 hour period and the nominal NO_2 detection range is 0.01 to 0.4 ppm (20 to 740 $\mu g/m^3$) of NO_2. However, the Environmental Protection Agency (EPA) approved method utilizes a 35 percent collection efficiency factor independent of the concentration of NO_2. It has been reported that actually the efficiency factor is concentration dependent and is generally higher than the constant value suggested by EPA.[5,6] The factor varies from 65.1 percent at 0.05 ppm to 35.0 percent at 0.215 ppm. Thus, the EPA recommendation gives erroneously high values of NO_2 in the usual concentration ranges (0.02 to 0.2 ppm). Because the efficiency factor is concentration dependent, a variation in the concentration during the sampling period makes the results very difficult to interpret.

Various other methods have been suggested for NO_2 and NO_x measurement which do not rely on a concentration dependent calibration factor. The Griess-Saltzmann method is a wet chemical method[1] similar to the Jacobs-Hochheiser technique. Air is bubbled into a solution of the Griess-Saltzmann reagent for 30 minutes and the color is allowed to develop for an additional 15 minutes. The NO_2 reacts with sulfanilic

acid to form a diazonium salt, which couples with N-1-napthyl-ethylenediamine dihydrochloride to form a deeply colored azo dye. The attenuation of light at 550 nanometers (nm) is proportional to the concentration of NO_2 in the air in the range 0.02 to 0.75 ppm (40 to 1500 $\mu g/m^3$). The drawback of this method is that samples must be analyzed within one hour of the sampling period. A description of these two wet chemical methods has been included to give an indication of the complexity of analyzing the results after the sampling is performed. Among other techniques which have been suggested as alternatives to the Jacobs-Hochheiser reference method are:

(1) a triple system for continuously measuring carbon monoxide, sulfur dioxide, and nitrogen dioxide based on the fuel cell principle;[7]

(2) a method for determining NO_X in which ozone is titrated in the gas phase with a reactive gas and the reaction produces light by chemiluminescence;[8]

(3) gas chromatography;[9]

(4) long-path infrared spectroscopy; and

(5) derivitive spectrophotometry.[10,11]

It is expected that the reference method for NO_2 will be changed by the EPA from the Jacobs-Hochheiser technique to the chemiluminescent method.

Several workers have pointed out the need for NO_X measurement devices which do not rely on the wet chemical methods involving treatment of samples.[2,7] Morgan,[7] and co-workers for the EPA, have commented about wet chemical methods:

> In the past, the operation of most mechanized and automatic analyzers has been based on wet chemical methods. These methods have inherent problems and are not entirely satisfactory for typical field applications because they must be attended frequently, reagents are unstable, and the instrumentation requires complex plumbing and accurate solution pumps with the result that the instruments are heavy and bulky. Future instruments hopefully will utilize the physical or physiochemical properties of pollutants for identification and quantification.

Based on the need for a direct measuring device, the decision was made to investigate optical techniques which could accurately and instantaneously measure normal urban concentrations of pollutants, and in particular, NO_2.

Optical Methods of Air Pollution Surveillance

Several optical methods have been suggested for the remote detection of air pollution: Raman backscattering, resonance Raman backscattering, resonance backscattering, and resonance absorption.[12] A summary of these techniques, which usually use lasers for light sources, is given below.

Raman spectra depend on the collision of incident light quanta with the molecule, where the molecule is induced to undergo a change in energy through a pure rotational, or a vibrational, or a rotation-vibration change. The corresponding emergent light quantum is altered in energy (and frequency) by this amount. The Raman effect depends on a changing polarizability during the vibration or rotation. The vibrational Raman shifted frequencies are specific and allow interference-free detection of many important pollutant molecules. The Raman technique employs a high power fixed frequency laser to

excite a large number of these transitions for the different molecules present in the atmosphere. The resonance Raman technique is similar except that a tunable frequency laser is employed so that the exciting frequency is nearly matched to an absorption frequency of a particular molecule. This increases the Raman cross section greatly for that molecule. The usual remote Raman technique[12,13] consists of a high power laser (tunable for the resonance technique) with the collection optics and electronics located at the Raman source. Thus, it is the backscattered Raman signal which is examined. The collected light is focused into a spectrometer (usually a double spectrometer) which separates the Raman shifted radiation from the backscattered light. The data must then be processed to identify the different molecules present. The Raman scheme has the advantages of depth resolution, and the fact that all the optics are in one location. It has the disadvantages of a lack of sensitivity (about 10 ppm at 100 m. with less sensitivity at greater distances),[12] and a requirement for sophisticated collection optics and data processing.

Resonance absorption and emission processes depend on a changing electric dipole moment of the molecule during the transition. Resonance backscattering requires the use of a tunable source which selectively excites various pollutants. After excitation, the excited molecule emits spontaneous radiation into a solid angle of 4π steradians. Monitoring the backscattered radiation determines the type of pollutants and their relative concentrations. This technique is similar in operation to the Raman method except that in electronic molecular excitations the backscattered fluorescence bands are sampled rather

than the Raman shifted radiation. This shift in wavelength for molecular excitations allows discrimination against Mie backscattering which is the limiting factor for atomic excitations where there is no wavelength shift. The resonance backscattering method for molecular electronic transitions gives some information on both the location and relative concentrations of the pollutants, but absolute concentrations are difficult to calculate. The system requires large collection optics and some data handling equipment.[12]

The resonance absorption scheme is based on the decrease in transmitted intensity when the light source is tuned to an absorption frequency for the pollutant. A tunable laser is used to tune across an absorption band, or a multiple-wavelength laser with wavelengths corresponding to both the absorption frequency and to non-absorbing frequencies is used. A comparison of the intensities at the absorbed and transmitted wavelengths gives a measure of the total integrated pollutant density in the beam path. The intensity measurements are made at a remotely located detector, or a retroreflector is employed to return the signal to the source location for measurement. This method has the advantages of high sensitivity, relative simplicity, and minimal beam powers. It has the disadvantages of no depth resolution, and a requirement for a retroreflector or a remote detector.

The absorption technique was selected for a feasibility study for the detection of NO_2 in the visible region. This method was selected because with its high sensitivity it appeared to be the only method capable of accurately measuring the normal urban NO_2 concen-

tration. The absorption of light by NO_2 was first studied using a tungsten lamp with a continuous output from 400 nm to 700 nm, with a monochrometer used for a wavelength filter. The resulting absorption spectrum displayed overlapping bands throughout the visible region (400 to 650 nm), with the strongest absorption in the deep blue-violet (400 to 460 nm) and becoming progressively weaker towards the red (above 600 nm). Based on this spectrum, two sources with discrete output wavelengths were selected as possible light sources for a NO_2 detection device. The absorption coefficients for the output wavelengths of these two sources, a mercury lamp and an argon-ion laser, were measured and the argon-ion laser was selected as the light source. The argon-ion laser has two output spectral lines which are separated in wavelength by only 5.2 nm, but differing in absorption coefficient by a factor of two. By comparing the relative strengths of these two lines after transmission through the atmosphere, it was thought to be possible to calculate the average NO_2 concentration in the light path of the laser. The mathematical theory for this calculation is presented in the next chapter.

CHAPTER II

MATHEMATICAL THEORY OF THE ABSORPTION TECHNIQUE

The purpose of this mathematical development is to show how measurable quantities such as light intensity, path length, and absorption coefficients can be used to determine the desired quantity - that is, the average atmospheric NO_2 concentration. Specific calculations are made for the output wavelengths of a TRW Instruments Model 71B pulsed argon-ion laser since this was selected as the light source for the NO_2 detection device. The output wavelengths for this laser are 476.5, 488.0, 496.5, 501.7, and 514.5 nm. In this chapter an equation relating the ratio of the transmitted intensities of two of these lines to the average NO_2 concentration is shown. The difference in the attenuation of these two wavelengths is due not only to a difference in absorption by NO_2, but also to wavelength-dependent scattering processes. The possibility of absorption by other gases is discussed in Chapter IV.

Gaseous Absorption of Light

The energy for an isolated molecule may be written as,

$$E = E_e + E_v + E_r + E_t \tag{4}$$

where E_e is the electronic energy, E_v is the vibrational energy, E_r is

the rotational energy, and E_t is the translational energy. The first three terms are quantized and take discrete values only. These values are specified by quantum numbers and the set of quantum numbers describes an energy state. For absorption and emission processes radiation interacts with molecules by causing a transition from one energy state to another, the frequency (ν) of the absorbed or emitted quantum being given by

$$E = h\nu \tag{5}$$

where h is Planck's constant, and E is the difference in energy between the two states. In absorption and emission processes, an atom or molecule interacts with electromagnetic radiation through its electric or magnetic dipole or quadrupole moments.

The least energetic transitions involve changes in the rotational energy of the molecule which give rotational spectral lines occurring in the microwave or far infrared region of the spectrum. Vibrational energy changes, involving changes in the vibrations between the atoms making up the molecule, are much larger than rotational ones and rotational changes usually accompany the vibrational changes. The resulting group of spectral lines for a single vibrational change, coupled with the several possible smaller rotational energy changes, forms a vibration-rotation band in the intermediate infrared spectrum. Electronic transitions involve electrons changing from one orbit (quantum state) to another which

results in even larger energy changes of a few electron volts. The electronic changes in molecules are always accompanied by changes in vibrational and rotational energy levels, which form complex spectral band systems in the visible and ultraviolet spectral region.

The absorption spectrum of nitrogen dioxide in the visible region is due to electronic transitions which give rise to a set of very complex overlapping band systems. This spectrum has been measured[14,15,16,17] and attempts have been made at theoretical explanations for some of the band systems,[14,15,18,19,20] but no satisfactory explanation of the complete visible range spectrum has yet been presented. Part of this investigation has involved measurement of the absorption of NO_2 in the visible region and calculation of absorption coefficients for specific wavelengths with better accuracy than has been previously reported.

Beer's Law, which describes light attenuation due to absorption, can be derived by considering a volume of absorbing molecules at concentration c. Let the attenuation (at a given wavelength) per unit concentration, per unit path length in the volume, per unit incident light intensity be given by σ. If the intensity is given by I and the path length by r, then the attenuation per unit length is

$$dI/dr = -I\sigma c. \qquad (6)$$

Rearranging and integrating the distance from zero to R, the total path length through the absorbing gas, and integrating I from I^o to I^R, the initial and final intensities, respectively, one gets,

$$\int_{I^o}^{I^R} dI/I = \int_{0}^{R} -\sigma c \, dr \tag{7}$$

$$\log_e(I^R/I^o) = -\sigma cR \tag{8}$$

$$I^R = I^o \exp(-\sigma cR). \tag{9}$$

Dropping the subscript R for the final intensity gives

$$I = I^o \exp(-\sigma cR) \tag{10}$$

which is Beer's Law. From the previous discussion, it can be seen that σ is a function of wavelength, the function being described approximately by a spectrophotometric spectrum of the substance of interest.

Scattering of Light

In addition to transmission losses due to gaseous absorption, the light signal propagating through the atmosphere is attenuated and scattered by other processes. The most important of these processes are those due to the lack of homogeneity in the density of the atmosphere. These processes are usually treated under three separate theories, with the distinction between the processes being made

on the relative size of the radiation wavelength to the extent of the inhomogeneous region of the atmosphere. The small inhomogeneous regions are usually molecules or particles while the larger regions could be masses of air differing in temperature or humidity. Rayleigh scattering governs the regime where the radiation wavelength is large relative to the particle or density inhomogeneity, while the Mie theory is used when the particle is of comparable size or larger than the wavelength. When the inhomogeneous volumes are masses of air much larger than the radiation wavelength, a classical calculation of the scattering (or refraction) due to refractive index fluctuations is used.

The Rayleigh scattering theory is derived from electromagnetic theory with the following assumptions:

(1) dimensions of the scattering particles are small relative to the wavelength (i.e., diameter less than 0.1 μm for visible light);

(2) the scattering particles and medium are not conductors;

(3) the dielectric constants of the particle and of the medium differ by a small value;

(4) the particles scatter light independently of each other.[21]

Along with these assumptions a spherical model for the scattering particle is used with a spatially uniform but time varying electric field applied. The interacting electric field causes the particle to radiate with a characteristic dipole radiation pattern. The scattered energy is proportional to the inverse of the fourth power of the exciting wavelength, and for atmospheric radiation attenuation,

Rayleigh scattering is most important in the ultraviolet region. For optical scattering most of the Rayleigh scatterers are molecules, so that Rayleigh scattering provides a fairly constant attenuation factor in time. The attenuation equation for Rayleigh scattering is similar to the one already shown for absorption, except that the Rayleigh coefficient β is used in place of product $c\sigma$, resulting in an equation of the form

$$I = I^{o} \exp(-\beta R) \tag{11}$$

where β is a function of wavelength. The Rayleigh attenuation coefficients at the wavelengths of the argon-ion laser used in this experiment are given in Table 1.

Both the theory and the physical processes involved in Mie scattering are considerably more complex than for the Rayleigh case. Among the processes involved in the complete Mie scattering are: dipole, quadrapole and higher order reradiation, surface reflection, refraction, internal reflection, surface waves, and diffraction. A complex mathematical theory has been developed for Mie scattering, but to apply it requires not only the use of cumbersome mathematics but also the distribution function of particle sizes. In the real atmosphere the size distribution is unknown and constantly changing. For this reason the atmospheric Mie scattering coefficient is usually estimated empirically. The following relation has been used in this paper to estimate the Mie scattering coefficient,[22]

Table 1. Comparison of the Attenuation Coefficients for Light Scattering Processes (Coefficients for Rayleigh scattering, Mie scattering (visibilities of 4, 10, and 15 km), and refractive index fluctuations are compared for the argon-ion laser wavelengths).

λ nm	Rayleigh[a] $\beta_\lambda \times 10^{4}, m^{-1}$	Mie[b] $\delta_\lambda \times 10^{4}, m^{-1}$ V = 4km	10km	15km	Refractive Index Fluctuations[c,d] γ_λ	$(\gamma_\lambda/R)\times 10^{4}, m^{-1}$
476.5	0.2122	11.168	4.6849	3.2060	0.51719	0.73049
488.0	0.1929	10.923	4.5461	3.0976	0.50300	0.71045
496.5	0.1800	10.749	4.4483	3.0214	0.49297	0.69629
501.7	0.1726	10.646	4.3902	2.9763	0.48701	0.68787
514.5	0.1561	10.400	4.2530	2.8701	0.47291	0.66795

a Calculated from $\beta_\lambda = \beta_{\lambda_o}(\lambda_o/\lambda)^4$, where $\lambda_o = 500$ nm, $\beta_{\lambda_o} = 0.1750 \times 10^{-4} m^{-1}$.

b Calculated from[22] $\delta_\lambda = (3.91/V)(550/\lambda)^{0.585} V^{1/3} \times 10^{-3} m^{-1}$ where V is the visibility in km and λ is the wavelength in nm.

c Calculated from $\bar{I} = I^o \exp(-\alpha(1/\lambda)^{7/6}) = I^o \exp(-\gamma_\lambda)$ where $\alpha = 6.887\ (nm)^{7/6}$ which derives its value from the measured result $(\bar{I}/I^o) = 0.623$ at $\lambda = 514.5$ nm.

d Since the path length R contribution to the total attenuation factor γ_λ is not linear as it is for the Rayleigh ($\beta_\lambda R$) and Mie scattering ($\delta_\lambda R$), an attenuation factor in units of R^{-1} can not be derived as in the other two cases. But to offer a comparison between the various attenuation coefficients, γ_λ can be divided by R for the particular path length used (R = 7080 m).

$$\delta = (3.91/V)(550/\lambda)^{0.585\ V^{1/3}} \times 10^{-3}\ m^{-1} \qquad (12)$$

where δ for Mie scattering is analogous to β for Rayleigh scattering in equation (11), and where V is the visibility in km and λ is the wavelength in nm. The attenuation equation for Mie scattering is just equation (11) with β replaced by δ. The magnitude of the Mie scattering depends on the amount of dust and aerosols in the atmosphere which is highly variable over a period of time. Thus, δ is a slowing varying function of time and has some wavelength dependence, but not as much as the Rayleigh $(1/\lambda)^4$ dependence. Mie scattering is larger than Rayleigh scattering in the visible region as is shown in the comparison in Table 1. The Mie attenuation coefficients are calculated for three visibility ranges - 4 km which is about the minimum operable visibility for the detection device, 10 km which is considered typical, and 15 km which is taken as a maximum value for this location.

Rapid fluctuations in the intensity of the atmospheric transmitted laser beam were observed, and were due to the refraction of light by large scale atmospheric density fluctuations due primarily to convective currents and wind shears. This refraction caused very rapid fluctuations with a magnitude of about 50 percent of the average transmitted intensity. While no measurements were made, there seemed to be some correlation between the magnitude of the fluctuations and wind turbulence and convective heating currents.

The large intensity variations observed at a fixed receiver seemed to be peculiar to the laser beam since conventional light sources located in the same area as the reflector showed much smaller intensity fluctuations (barely noticable to the human eye). The problem of large scale turbulence effects has been studied in connection with stellar scintillation[23,24] and recently several workers have recorded and offered various explanations of the laser scintillations.[25,26,27] The process of laser beam scintillation is not completely understood at present, but two probable reasons for the laser beam intensity fluctuations being larger than those of conventional sources are the following. First, the laser beam is well collimated into a very small cone which can easily be refracted from the original direction, while a conventional source radiates into a sphere, or, if focused in a particular direction, into a much larger cone than the laser beam. Secondly, the laser beam initially has transverse coherence which can be modified to some arbitrary pattern by the differences in refractive index along the beam path. This gives rise to off-axis interference effects causing angular scintillations in the beam trajectory.[25] Wohlers[26] gives the following approximation for attenuation of a laser beam due to turbulence.

$$\bar{I} = I^{o} \exp(-3.12\ (2\pi/\lambda)^{7/6} R^{11/6} C_N^2) \qquad (13)$$

where $\bar{I}$ is the average transmitted beam intensity, I^{o} is the intensity transmitted without turbulence effects, λ is the radiation

wavelength, R is the path length, and C_N^2 is a measure of the strength of the turbulence. No values are given by Wohlers for C_N. A rough approximation of C_N for a typical day with the setup used in this experiment gave $C_N = 10^{-8} m^{-1/3}$ for the 514.5 nm argon-ion line. The average attenuation due to density fluctuations was estimated to be 38 percent for the 514.5 nm line. Of particular importance for the NO_2 detection device was the difference in attenuation coefficients rather than the absolute values for the five argon-ion wavelengths. To estimate the attenuation coefficients at the different wavelengths, the above values for the 514.5 nm line are used along with the wavelength dependence given by Wohlers. The above attenuation equation can be rewritten in terms of a constant factor α and the wavelength dependence $(1/\lambda)^{7/6}$ or in terms of a single wavelength dependent coefficient $\gamma_\lambda = \alpha(1/\lambda)^{7/6}$,

$$\bar{I} = I^o \exp(-\alpha(1/\lambda)^{7/6}) = I^o \exp(-\gamma_\lambda) \qquad (14)$$

where $\alpha = 3.12(2\pi)^{7/6} R^{11/6} C_N^2$. The value for α can be solved for from the data given above for the 514.5 nm line, and then the attenuation coefficients γ_λ can be solved for from the given wavelength dependence. The resulting values for γ_λ for the argon-ion wavelengths are shown in Table 1. It should be noted that in comparing γ_λ with the coefficients for Rayleigh and Mie scattering, the total path length dependence in the attenuation coefficient is $R^{11/6}$ as opposed to the linear relation for Rayleigh and Mie scattering. To give some

comparison between the coefficients, γ_λ/R is shown in addition to γ_λ. Caution must also be used in interpreting these refractive index fluctuation coefficients because they are representative of the particular experimental apparatus used and are not generally valid for other experiments.

Among the experimental factors affecting the intensity fluctuations as measured in the transmitted laser beam are the size of the reflector and receiving optics, and the proximity of the receiving optics to the output optics. An increase in the size of the reflector and receiving optics should decrease measured fluctuations because more of the angular deviations of the beam are received and recorded. This has been verified in stellar observations.[23] In this experiment some improvement in stability of the intensity of the return beam was noticed when the effective receiving aperture was increased from 25 mm to 102 mm, but not as much improvement as was expected. Also to decrease fluctuations, the distance between the outgoing laser beam axis and the optic axis of the receiving lens should be kept as small as is practical.

Total Attenuation of Light in the Atmosphere

The attenuation equations for the absorption process and the three scattering processes can be combined into one equation expressing the transmitted intensity at a given wavelength λ as,

$$I_\lambda = I_\lambda^o \exp(-(\sigma_\lambda c R + \beta_\lambda R + \delta_\lambda R + \gamma_\lambda))$$

where σ_λ is the absorption coefficient, β_λ is the Rayleigh coefficient, δ_λ is the Mie coefficient, and γ_λ is the refractive index coefficient. It would be very difficult to use this equation alone to determine the concentration c of the absorbing gas for two reasons. First the coefficient γ_λ for refractive index fluctuations is only an average factor, while the attenuation varies rapidly with time. Secondly, because of the divergence of the laser beam, only a small portion of the beam is intercepted and detected by the optics and electronics, so I^o is very much less than the output intensity of the laser. However, if the ratio of the transmitted intensities of two lines of slightly different wavelength but large differences in absorption coefficient is measured, then only the ratio of the two I^o's needs to be computed and this is very close to the same as the ratio of the intensities at the laser. This ratio method also allows for the cancellation of most of the scattering effects and thus enhances the effects of the absorption process. The mathematics of this ratio technique are shown below where the symbol a is the wavelength for the strongly absorbed line and b is the wavelength of the weakly absorbed line.

$$I_a = I_a^o \exp(-(\sigma_a cR + \beta_a R + \delta_a R + \gamma_a)) \qquad (16)$$

$$I_b = I_b^o \exp(-(\sigma_b cR + \beta_b R + \delta_b R + \gamma_b)) \qquad (17)$$

Taking the $\log_e$ of both sides of both equations,

$$\log_e(I_a/I_a^o) = -(\sigma_a cR + \beta_a R + \delta_a R + \gamma_a) \qquad (18)$$

$$\log_e(I_b/I_b^o) = -(\sigma_b c R + \beta_b R + \delta_b R + \gamma_b) \ . \qquad (19)$$

Subtracting the first from the second, one gets,

$$\log_e(I_b/I_b^o) - \log_e(I_a/I_a^o) = (\sigma_a - \sigma_b)cR + (\beta_a - \beta_b)R \qquad (20)$$

$$+ (\delta_a - \delta_b)R + (\gamma_a - \gamma_b).$$

From the properties of logarithms,

$$\log_e(I_b/I_b^o) - \log_e(I_a/I_a^o) = \log_e(I_a^o/I_b^o) - \log_e(I_a/I_b). \qquad (21)$$

Solving for the concentration c,

$$c = (1/((\sigma_a - \sigma_b)R))(\log_e(I_a^o/I_b^o) - \log_e(I_a/I_b) - (\beta_a - \beta_b)R \qquad (22)$$

$$- (\delta_a - \delta_b)R - (\gamma_a - \gamma_b))$$

where all values are known or measurable, or can be estimated, except for c , the concentration, and the absorption coefficients which are presented in the next chapter. After values for the absorption coefficients are obtained, it can be ascertained what the limitations are

in the detection of nitrogen dioxide due to variations in the other attenuation parameters. One assumption which has been made is that the fluctuations of the two lines due to refractive index changes in the atmosphere will occur in phase, and thus most of these fluctuations could be subtracted out by using some type of ratio technique.

CHAPTER III

MEASUREMENT OF THE ABSORPTION SPECTRUM OF NITROGEN DIOXIDE IN THE VISIBLE REGION

Introduction and Previous Work

The absorption of nitrogen dioxide in the visible range of the spectrum has been previously studied. However, Pearse and Gaydon[17] report the location of some of the strong edges and maxima only. Douglas and Huber,[14] and Robinson, McCarty, and Keelty[15] presented their results in the form of photographs of spectrograms, from which absorption coefficients cannot be calculated. The work of Dixon[16] includes curves resulting from spectrophotometric measurements and the absorption coefficient for NO_2 in the visible region, but it lacks the detailed measurements necessary for this study. The main purpose of Dixon's work was to measure the trend of the average absorption coefficient across the visible region and the spacing between the minima. Since no previous work had been done to the accuracy needed for this experiment, it was determined that the absorption coefficient of NO_2 across the visible spectrum should be measured.

The experimental apparatus which was used to do this absorption study is shown in Figure 1. Actually three separate experiments were performed using this same apparatus except for a change in light sources. First, the absorption spectrum of NO_2 across the entire visible range was measured using a tungsten lamp source. Based on the results of this

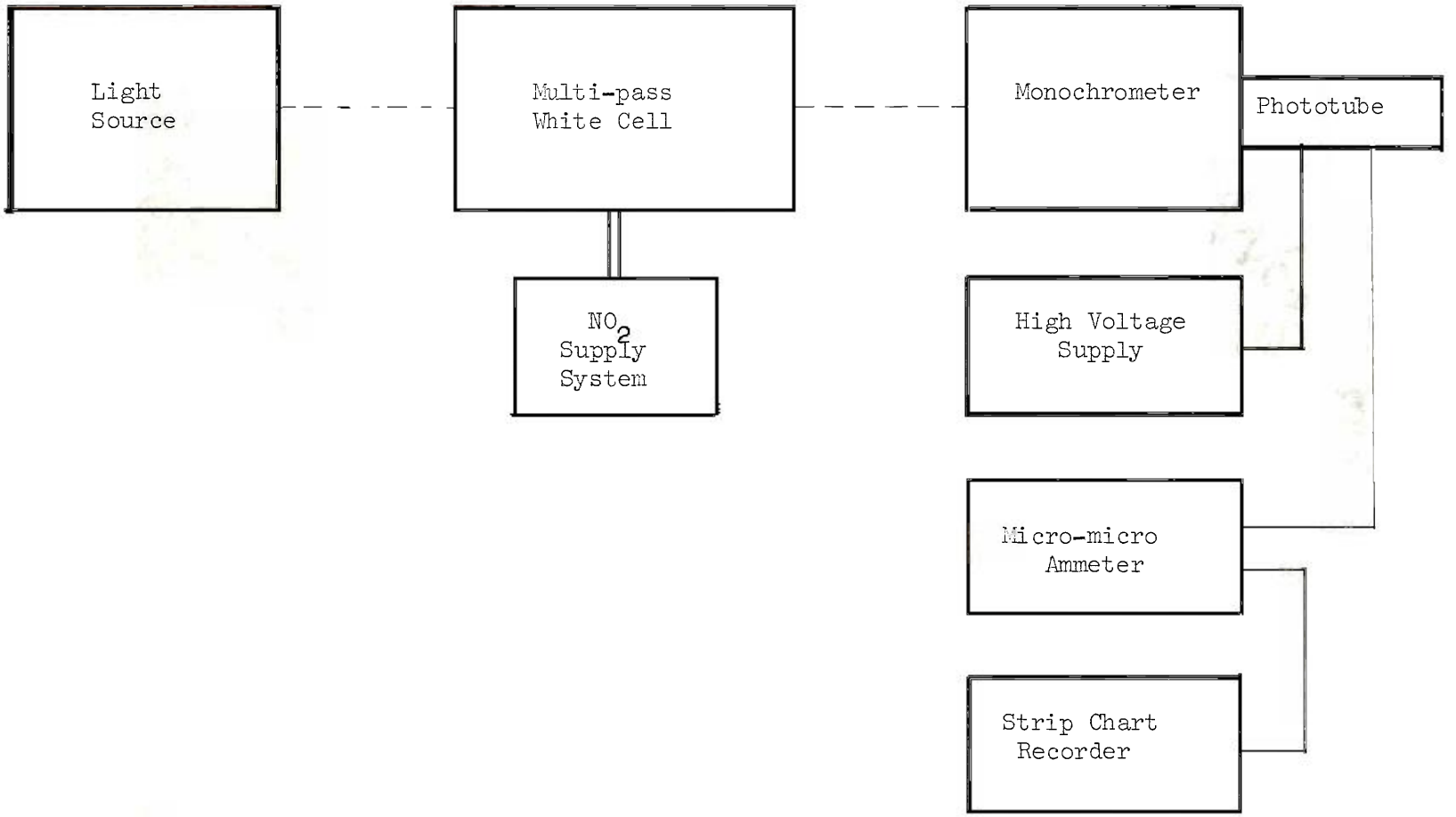

Figure 1. Apparatus for the Measurement of Light Absorption by NO_2.

spectrum, a mercury lamp and an argon-ion laser were selected as possible light sources for a NO_2 detection device. The absorption coefficients for the discrete output wavelengths of these two sources were then measured using the same apparatus as was used for the complete spectrum measurement.

A description of the experimental apparatus and procedures which were used, and the results obtained for these three experiments are presented in this chapter. In the first section the calibration for the amount of nitrogen dioxide in the sample cell is presented, then the optical layout is explained, and finally the results for all three light sources are presented and compared with results of previous workers.

Determination of the Nitrogen Dioxide Concentration in the Multi-pass Cell

The nitrogen dioxide supply system was mounted on the cart supporting the multi-pass White cell which was used to provide a long sample path length with good absorption at a low NO_2 pressure. A lecture bottle of liquid nitrogen dioxide (minimum of 99.5 percent purity) obtained from the Matheson Company was used without further purification. The gas was removed at the vapor pressure of the liquid (approximately 1.08 atmospheres (atm)) and was then channeled through a supply network and into the White cell. The supply network was assembled from stainless steel and aluminum tubing and cast iron pipe fittings, and Whitey stainless steel valves were used to control the flow. The procedure used to allow a measured amount of NO_2 into the

White cell was as follows: the NO_2 vapor was allowed to pass through a valve and into an evacuated volume, called V_a, of 11.2 milliliters (ml). After equilibrium was established, the valve to the NO_2 tank was closed and the valve separating the small volume V_a from the evacuated White cell was opened. This allowed a measured amount of NO_2 to be released into the White cell where its pressure was reduced by a factor of about 10^4. This process could be repeated several times with very close to the same amount of NO_2 admitted each time. There was also an additional empty lecture bottle which was connected to the smaller volume V_a and which could be evacuated and used to dilute the NO_2 gas at about atmospheric pressure in V_a to a much lower pressure. Thus, when the valve to the dilution lecture bottle was opened and then closed before the NO_2 in V_a was bled into the White cell, a considerably smaller amount of NO_2 would enter the White cell. This extra dilution step was not used except to check the apparatus for very small concentrations of NO_2. The volume of the White cell was 131 liters and the volume of V_a was 11.2 ml giving a ratio of the volumes of 8.56×10^{-5}.

A Welch Duo-Seal vacuum pump was used to evacuate the system and its exhaust was vented directly to the outside atmosphere. After NO_2 was added to the White cell, the vacuum pump was not used to exhaust the gas. Instead, the NO_2 was removed from the cell by connecting the exhaust line to the outside directly to the cell. Then dry nitrogen was bled into the cell through the other valved inlet until atmospheric pressure was reached. At that point, the valve to the exhaust line was opened and the cell was purged with dry nitrogen. After most of

the NO_2 was removed, the vacuum pump was reconnected and used to remove the remaining nitrogen and NO_2.

The White cell used could not be considered an excellent vacuum-tight unit. Because of the size of the O-ring seal (circumference of 325 cm), it was difficult to vacuum seal the whole unit, and consequently the best vacuum to which the cell could be pumped was about 20 microns of mercury (μmHg). It is believed that this did not affect the results except that accurate pressure measurements were made difficult by a small pressure rise when the pump was not connected.

Pressure measurements were taken with a NRC Model 801 thermocouple vacuum gauge meter and a NRC Model 531 thermocouple gauge. Later these were checked against the readings measured with a MKS Baratron Pressure Meter Type 77 and MKS Head 77H-1, 1 mmHg.

In order to calculate the absorption coefficients it was necessary to know the amount of NO_2 which had been admitted into the White cell. As a first approximation this could be calculated from the ideal gas law $PV = nRT$ and the known values for the pressures and volumes. That is, when the NO_2 is bled into the known small volume V_a, equilibrium pressure is reached at the vapor pressure of the liquid in the NO_2 supply cylinder which is a known function of the temperature.[28] The temperature of the liquid and the gas are assumed to be the same with both at room temperature. Thus, known values of P, V, T, and the gas constant, R, can be used to calculate n, the number of moles present. When the NO_2 in V_a is allowed to expand into the evacuated White cell, this same number of molecules n should

be present.

Measurements with the thermocouple gauge indicated pressures of the NO_2 in the White cell much higher than would be expected from the ideal gas law. From the ratio of the volume of V_a to the White cell, one unit of dry air, obeying the ideal gas law, caused a pressure rise of 65 μmHg when admitted into the evacuated White cell. ("One unit" means one volume of gas in V_a.) However, when the same volume of NO_2 in V_a at slightly higher initial pressure (1.08 atm instead of 1.00 atm because of the vapor pressure of the liquid) was added to the White cell, the indicated pressure on the thermocouple gauge was over twice that observed for air. This is due to two effects in addition to the higher initial pressure. The first is the difference in thermal conductivities of NO_2 and air which affects the operation of the thermocouple gauge. The second is that the number of molecules in the volume V_a was <u>not</u> the same as the number in the White cell; at higher pressures most of the NO_2 exists as the dimer N_2O_4 which dissociates into two molecules of NO_2 at the lower pressures in the White cell. Because the absorption was proportional to the number of NO_2 molecules, it was necessary to determine the amount of dissociation of N_2O_4 into NO_2 for both V_a and the White cell.

The detailed dissociation calculations are given in Appendix A. The results of these calculations are that 13.4 percent of the N_2O_4 in V_a is dissociated into NO_2 while in excess of 99.8 percent in the White cell is dissociated. For simplicity, it will be assumed that only NO_2 molecules exist in the White cell. From the above figures

it is shown in Appendix A that when the mixture of N_2O_4 and NO_2 is allowed to fill V_a at 1.08 atm and then is bled into the White cell, the resultant NO_2 pressure is calculated to be 124 μmHg. This 124 μmHg pressure of NO_2 is equivalent to a concentration of 164 ppm at atmospheric pressure; that is, if the 124 μmHg of NO_2 were diluted with another gas at atmospheric pressure, the resulting NO_2 concentration would be 164 ppm.

This value for the pressure was compared to the experimental value by the use of a diaphragm type pressure gauge - a MKS Baratron Pressure Meter Type 77 with a MKS Head 77H-1, 1 mmHg. Although it was difficult to get an accurate measurement with this gauge because of a small leak in the White cell, the mechanical gauge gave a reading of about 131 μmHg which verified the 124 μmHg pressure value resulting from the dissociation calculations. Thus, the 124 μmHg was accepted as a close estimate of the real NO_2 pressure rise in the White Cell when one unit of V_a was bled into the cell.

The Optical System

The layout of the optical system can be seen in Figure 1. The output of the light source is focused into the multi-pass White cell where the absorption by the NO_2 gas occurs. The amount of transmitted light as a function of wavelength is measured by the monochrometer and phototube, and is recorded by a strip chart recorder after amplification by a micro-micro ammeter.

Three light sources were used in the absorption experiments. The entire absorption spectrum across the visible region was measured

using a 50 watt tungsten lamp with a frosted glass bulb for the light source. Then the absorption coefficients at the discrete output wavelengths of a mercury lamp (Atomic Laboratories Cat. No. 71859) and an argon-ion laser (TRW Instruments Model 71B) were measured.

The theory and construction of White cells is discussed in detail by White.[29] The essential parts of the system are three identical spherical concave mirrors, in this case, mirrors 25.4 cm in diameter with a radius of curvature of 80 cm. These are positioned as shown in Figure 2. The centers of curvature of mirrors A and A' are at the front surface of B, and the center of curvature of B is halfway between A and A'. The number of passes is adjustable by symmetrically moving mirrors A and A' such that their centers of curvature change separation distance while their midpoint remains centered in mirror B. As the separation of the centers of curvature of A and A' is decreased, the number of passes is increased from 5 to 9, 13, 17, . . . $4n + 1$, where n is a positive integer. The maximum number of passes for this White cell was 41 resulting in a path length of 33.06 m, but 17 passes (13.86 m) were used for the tungsten lamp and mercury lamp spectra, and 5 passes (4.26 m) were used for the argon-ion spectrum. Optical access through the stainless steel White cell was obtained through three glass window ports sealed with O-rings.

After the beam traversed the White cell, it was focused by a 4 cm focal length lens onto the entrance slit of a Jarrell-Ash Model 82-410 0.25 meter monochrometer. The monochrometer grating could be rotated with an electric motor to give a linear relation

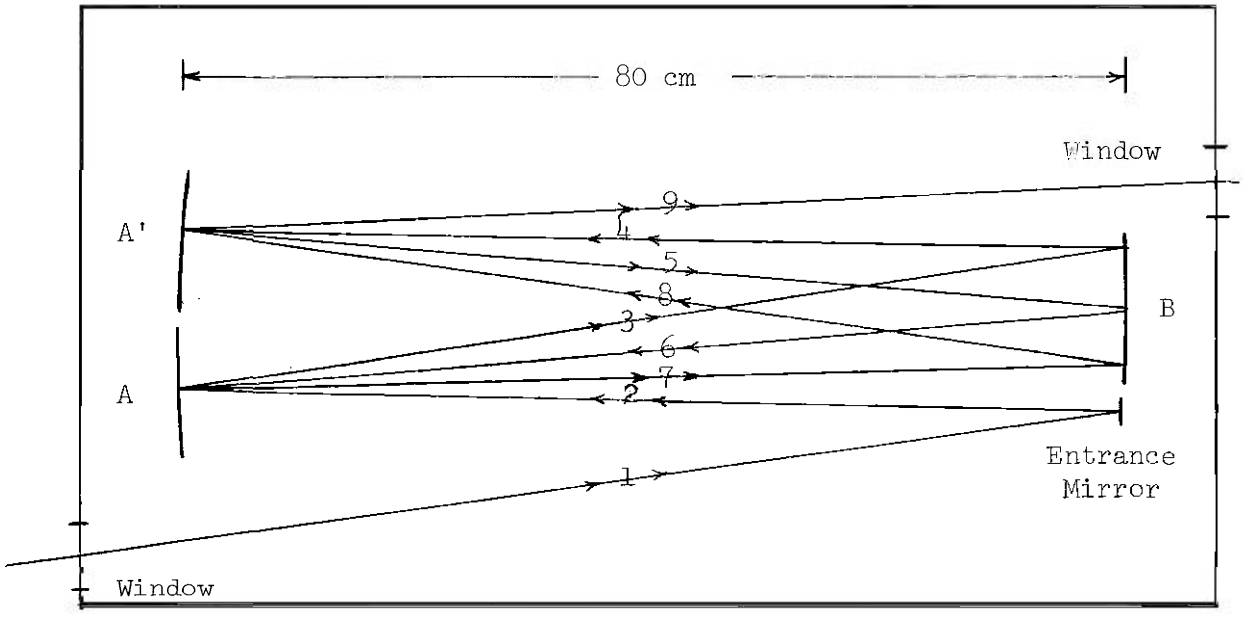

Figure 2. The Multi-pass White Cell. (Mirrors set for 9 passes)

between wavelength and time. The 1 rotation per minute (rpm) motor resulted in a 25 nm per minute scanning rate across the exit slit. Both the input and exit slits were 100 μm in width giving a resolution of 0.5 nm.

A RCA 1P28 multiplier phototube was mounted to the monochrometer at the exit slit. A voltage of about 750 volts was supplied to the phototube by a Harrison Model 6515A DC Power Supply. Special precautions were taken when measuring the light intensity from the pulsed argon-ion laser to assure that the phototube stayed in the linear operating range. With the bleeder resistance used (0.8 M ohm/stage), the phototube linearity was restricted in that the current through the dynode-anode chain had to be small relative to the current in the bleeder string of resistances to keep a constant voltage drop between the dynodes. For a voltage drop of 80 volts across each of the nine dynodes and from the last dynode to the anode (total voltage of 800 v.), the current in the bleeder resistances was 0.1 milliampere (mA) which meant that the current through the anode was restricted to about one-tenth of that value or less than 10.0 microamperes (μA). The full scale setting on the micro-micro-ammeter was 0.3 μA for the tungsten lamp and the mercury lamp which was in the linear region of the tube. However, since the argon-ion laser was pulsed and the current in the phototube followed the actual pulse, this peak current had to be limited to less than 10.0 μA which restricted the average current registered by the ammeter to less than 0.022 μA (for a laser duty cycle of 0.22×10^{-2}). Neutral density filters of no. 2.0 and 4.0

were used in combination to cut the intensity of the laser beam by 10^6 to assure that the tube would operate in the linear region.

Absorption Spectra and Coefficients for Nitrogen Dioxide

The visible absorption spectrum of NO_2 was measured using the multireflection White cell set for a path length of 17 passes or 13.86 m. The White cell and the volume V_a were first evacuated and a spectrum of the tungsten lamp was taken with no NO_2 present. Then one unit of NO_2 in V_a was bled into the cell causing a pressure rise of 124 μmHg, equivalent to a concentration of 164 ppm at atmospheric pressure. After the light traversed this 164 ppm (equivalent) for a path length of 13.86 m, the spectrum was scanned by the monochrometer at 25 nm per minute. The resulting spectrum is presented in Figure 3, along with the spectrum of the light source with no NO_2 in the cell.

Values of the absorption coefficient may be calculated from Figure 3 for various wavelengths by use of equation (10),

$$I = I^{o}\exp(-\sigma cR) \qquad (10)$$

---

a Almost all of the strong absorption peaks reported by Pearse and Gaydon[17] for the visible region of NO_2 can be seen in Figure 3. Among these, and using the wavelengths quoted by Pearse and Gaydon, are 427.0, 430.4, 435.0, 439.0, 444.8, 448.0, 458.0, 463.0, 474.0, 479.5, 488.0, 494.5, 502.7, 504.8, and 509.5 nm.

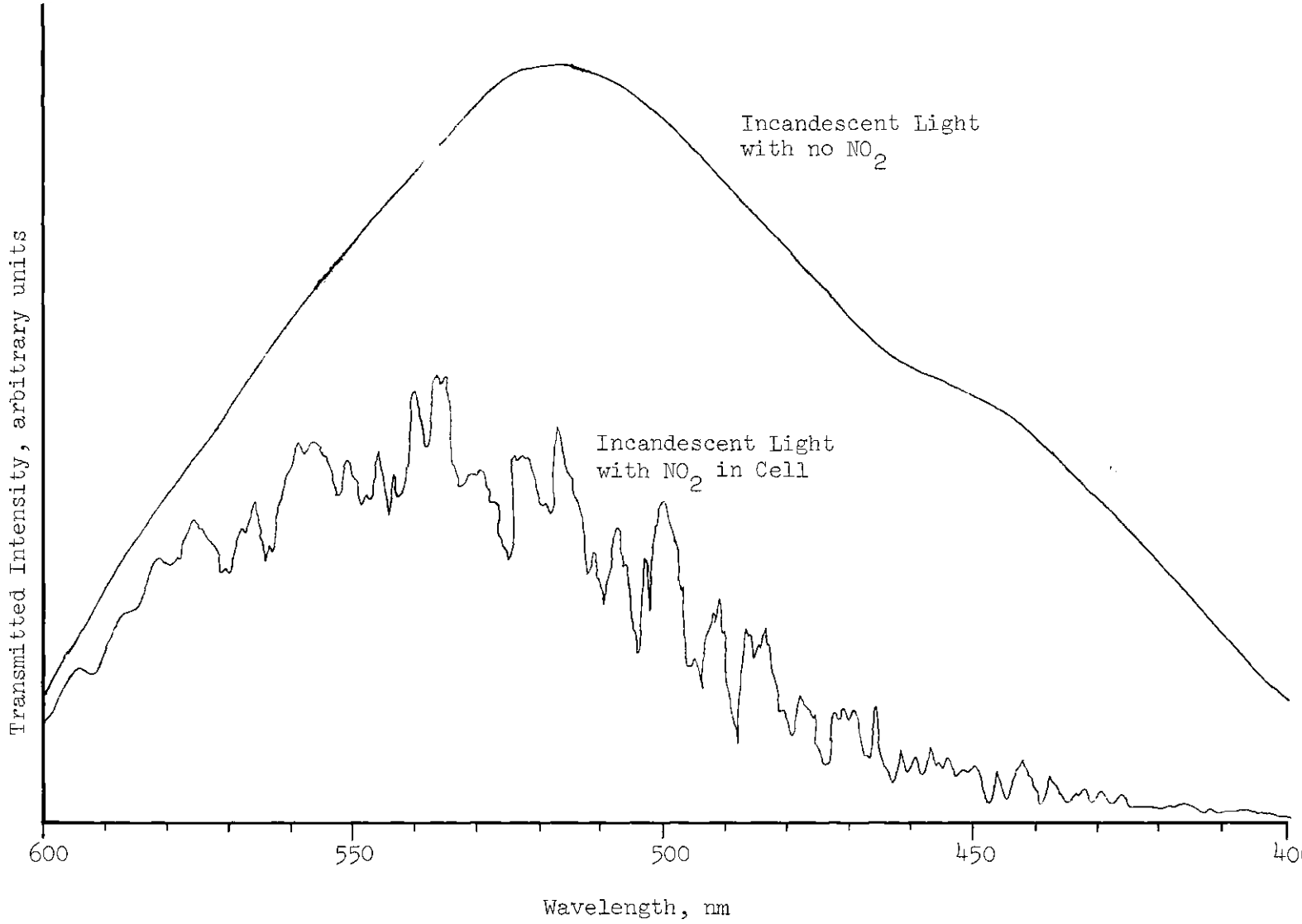

Figure 3. NO_2 Absorption in the Visible Region.

$$\sigma = (1/cR) \log_e (I^o/I) \qquad (23)$$

where σ is the absorption coefficient in $(\mu mHg)^{-1}m^{-1}$ or in $(ppm)^{-1}m^{-1}$, c is the pressure or equivalent concentration in the cell and is 124 μmHg or 164 ppm, R is the path length and is 13.86 m, I^o is the intensity transmitted with no NO_2 present, and I is the intensity with the NO_2 present.

The absorption spectrum presented in Figure 3 is actually the convolution of the real spectrum with the slit function of the monochrometer. Thus the detail observed in the spectrum increases with increases in the resolution of the optics until the resolution approaches the line width of the gas being measured. The line width for NO_2 under the experimental conditions used in measuring the spectrum is calculated in Appendix B. A brief description of line broadening is included below, along with the results of calculations shown in Appendix B.

Quantum theory states that the frequency of an absorption process is $\nu = (E_f - E_i)/h$ and the corresponding wavelength is $\lambda = c/\nu = hc/(E_f - E_i)$, where ν is the frequency of the radiation, λ is the wavelength, c is the velocity of light, h is Planck's constant, E_i is the energy of the initial state, and E_f is the energy of the final state. This would seem to indicate that only a single precise value of λ as defined above would be absorbed for any given transition, but in reality absorption lines and lines making up molecular bands have finite width. This broadening of the spectral lines about the

theoretical wavelength (or frequency) is due to several factors which are independent of the resolution of the measuring apparatus:

(1) the finite life of the excited state causes an uncertainty in the energy and a spread in the frequency due to the uncertainty principle;

(2) Doppler shifts in frequency due to relative thermal velocities of molecules;

(3) perturbations due to collisions of the absorbing molecule with similar and dissimilar molecules.

Order of magnitude estimates for the line broadening due to these three processes are made in Appendix B and the results are presented in Table 2. It can be seen in Table 2 that at the low pressure in the White cell, Doppler broadening dominates over pressure broadening and natural line width and results in a line width of about 10^{-3} nm.

The monochrometer which was used has a resolution of 0.5 nm, so there is a great deal of structure in the spectrum which has been averaged out by the monochrometer. An increase in resolution by a factor of 500 would be required to record all the variations in the spectrum. This increase in structure with a high resolution instrument is shown dramatically by McNamara[30] in a comparison of the absorption spectrum of SF_6 as measured by a grating spectrometer with a resolution of 0.07 cm^{-1} and a tunable diode laser with a resolution of 3×10^{-6} cm^{-1}.

The absorption coefficient calculated for any wavelength λ by an instrument with resolution $\Delta\lambda$ is given approximately by,

Table 2. Line Broadening for NO_2. (Estimates of line broadening of NO_2 absorption lines at 200 μmHg pressure and a temperature of 22.8° with a wavelength of 500 nm)

Line Broadening Process	Line Width Between Half Intensity Points (Order of Magnitude)	
	nm	cm^{-1}
Natural line broadening	0.5×10^{-6}	0.2×10^{-4}
Doppler broadening	10^{-3}	0.04
Pressure or collisional broadening	0.2×10^{-7}	10^{-6}

$$\bar{\alpha}_{\lambda} = \int_{\lambda - \frac{\Delta\lambda}{2}}^{\lambda + \frac{\Delta\lambda}{2}} \alpha(\lambda')\, d\lambda' \qquad (24)$$

where $\alpha(\lambda')$ is the actual absorption coefficient and $\bar{\alpha}_{\lambda}$ is the measured average coefficient. Thus the absorption coefficients for narrow line sources such as low pressure vapor lamps and lasers can only be estimated by the average absorption coefficient over a range of wavelengths when calculated from spectrum for continuous sources, such as the one given in Figure 3.

The spectrum presented in Figure 3 was used to select line sources (discrete output wavelengths instead of a continuous output) which, because of apparent large differences in absorption coefficients of their output wavelengths, could be used in an NO_2 detection device. It was then necessary to more accurately determine the absorption coefficients for the output wavelengths of these sources by direct measurement, since the line widths of the sources were less than the resolution of the monochrometer. The sources selected were a mercury vapor lamp, chosen for the great difference in absorption between the 435.8 nm and the 546.1 nm lines, and an argon-ion laser, selected for the difference in absorption of two lines close in wavelength - the 496.5 nm line and the 501.7 nm line.

The apparatus and procedure used in measuring the NO_2 absorption of the spectral lines of a mercury lamp were similar to those used for the continuous wavelength source. The tungsten lamp was replaced

by a mercury vapor lamp (Atomic Laboratories Cat. No. 71859) and the same path length of 13.86 m was used in the White cell. The ultraviolet output of the lamp was blocked by the use of a glass filter. Instead of bleeding all of the gas in V_a into the White cell at once, the valve to the White cell was quickly opened and closed twice before finally letting all the gas into the White cell. Before any gas was let into the cell, a spectrum was taken, and then each time after the valve was opened a spectrum was taken. This allowed the transmitted intensities to be measured at four different NO_2 pressures, the pressures being monitored by corrected readings from the thermocouple gauge.

The resulting transmitted intensities as a function of the NO_2 pressure in the cell are shown in Figure 4 and the absorption coefficients are presented in Table 3. The linearity of the points in Figure 4 shows that Beer's Law was obeyed for this experiment.

The experimental apparatus and procedures for studying NO_2 absorption of the argon-ion laser spectral lines were similar to those used for the other two light sources. A TRW Instruments Model 71B pulsed argon-ion laser was used as the light source and the path length of the cell was changed to five passes or 4.26 m. The procedure was changed so that four units of NO_2 in V_a of 124 μmHg each were added to the White cell, and the line intensities were measured before any NO_2 was added and then after each unit was added. The resulting percent transmission for the five different wavelengths as a function of NO_2 pressure is given in Figure 5 and the absorption

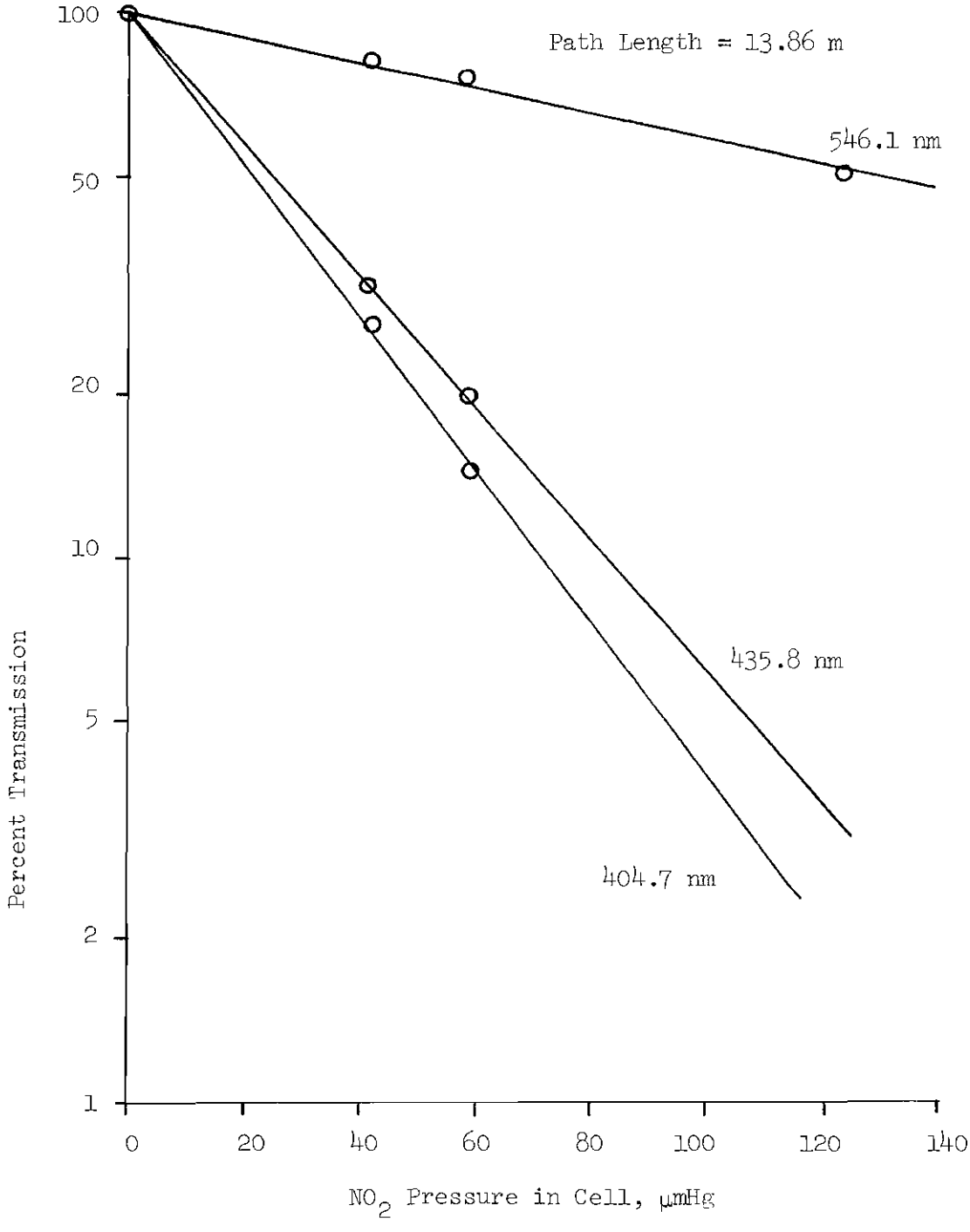

Figure 4. NO_2 Absorption at Mercury Lamp Output Wavelengths.

Table 3. NO_2 Absorption Coefficients at Mercury Lamp Output Wavelengths. (These were measured with a mercury lamp)

Wavelength	Absorption Coefficients[a]	
λ, nm	$\sigma \times 10^2$ $(mmHg)^{-1}\ cm^{-1}$	$\sigma \times 10^3$ $(ppm)^{-1}\ m^{-1}$
404.7	2.32	1.76
435.8	2.02	1.53
546.1	0.391	0.296

[a] Both sets of coefficients given in terms of a base *e* absorption equation. To convert to base 10 equation coefficients, divide by $\log_e 10 = 2.30$.

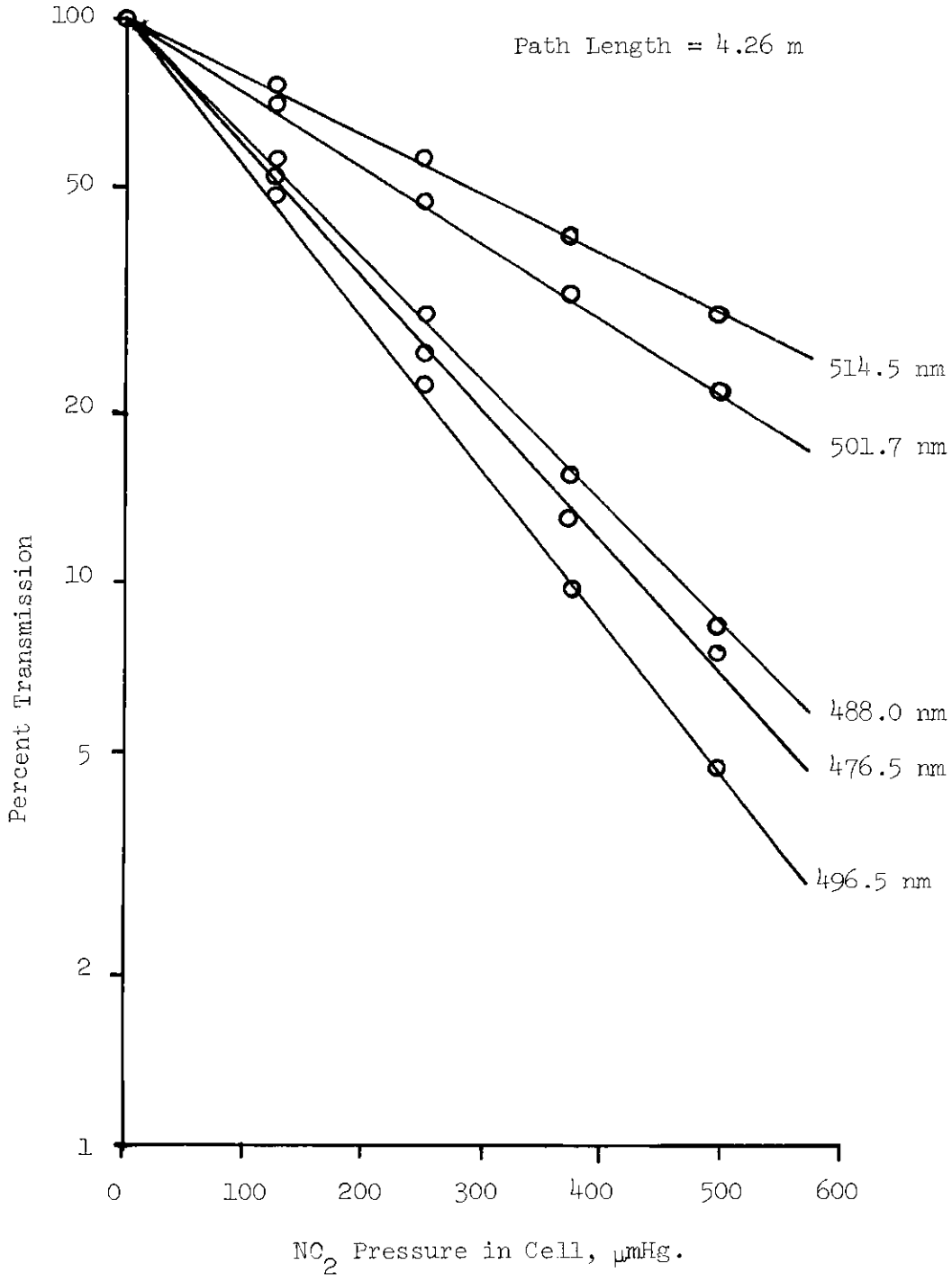

Figure 5. NO_2 Absorption at Argon-ion Output Wavelengths.

coefficients are presented in Table 4. The data points are an average of two runs, and their linearity shows that Beer's Law was followed for these experimental conditions.

A comparison of the absorption coefficients for the three light sources measured for this report with those reported by Dixon[16] is given in Table 5. It should be noted that the instrument resolution used by Dixon in studying the absorption of light from a tungsten lamp was 4 nm, while the resolution in this work was 0.5 nm. From the previous discussion on line widths and instrument resolution, it should be clear that because of the differences in resolution, some differences in spectrum structure and resulting absorption coefficients are to be expected. The absorption coefficients as computed by Dixon were generally higher than those reported here, particularly for the transmission peaks, but overall there was good agreement considering the difference by a factor of 8 in the instrument resolutions. The emphasis of the experiment resulting in Figure 3 was qualitative rather than quantitative and this should be kept in mind when computing coefficients from the spectrum of Figure 3. The coefficients given for the argon-ion laser are believed to be accurate as precautions were taken to insure quantitative accuracy.

Table 4. NO_2 Absorption Coefficients at Argon-ion Laser Output Wavelengths.

Wavelength λ, nm	Absorption Coefficients[a] $\sigma \times 10^2$ $(mmHg)^{-1}cm^{-1}$	$\sigma \times 10^3$ $(ppm)^{-1}m^{-1}$
476.5	1.26	0.954
488.0	1.15	0.875
496.5	1.46	1.11
501.7	0.716	0.543
514.5	0.565	0.428

[a] Both sets of coefficients given in terms of a base e absorption equation. To convert to base 10 equation coefficients, divide by $\log_e 10 = 2.30$.

Table 5. Comparison of NO_2 Absorption Coefficients. (The absorption coefficients for NO_2 as measured in this work for 8 near different sources are compared with those reported by Dixon.[16])

Wavelength λ, nm	Line Type[a]	Light Source	Absorption Coefficient[b] $\sigma \times 10^2$ $(\text{mMig})^{-1}\text{cm}^{-1}$		$\sigma \times 10^3$ $(\text{ppm})^{-1}\text{m}^{-1}$	
			Dixon	This Work	Dixon	This Work
433.9-435.8	M	mercury	2.25		1.70	
435.8	M	mercury		2.02		1.53
435.9	M	mercury	1.91		1.45	
441.5	T	tungsten	1.74	0.985	1.32	0.820
448.0	A	tungsten	1.91	1.81	1.45	1.37
488.0	A,L	argon laser		1.15		0.875
488.0	A,L	tungsten		1.16		0.877
491.0	A	tungsten	1.18		0.894	
500.0	T	tungsten	0.855	0.458	0.647	0.347
514.5	L	argon laser		0.565		0.428
514.5	L	tungsten	0.726	0.487	0.550	0.369

[a] Code for line type: A is absorption peak in spectrum, T is transmission peak, M is output wavelength of mercury lamp (but not necessarily with mercury lamp as source - see source column), and L is argon-ion laser output wavelength.

[b] For both sets of units, the coefficients are given in terms of a base e absorption equation instead of base 10 as used by Dixon. Divide by $\log_e 10 = 2.30$ to convert to base 10.

CHAPTER IV

MEASURING NITROGEN DIOXIDE CONCENTRATION IN THE REAL ATMOSPHERE

Application of the Attenuation Equation

After calculating the absorption coefficients of NO_2 for the argon-ion laser wavelengths and estimating the attenuation due to scattering effects at these wavelengths, the concentration of NO_2 in the atmosphere can be calculated by making several measurements. In order to calculate the concentration, the initial intensity ratio and the transmitted intensity ratio must be measured and the path length must be known. The values for these measurable quantities and for the attenuation coefficients can be used in equation (22) to calculate the average NO_2 concentration in the laser beam path.

A graph of the concentration as a function of the transmitted intensity ratio can be constructed once the fixed values of the initial intensity ratio and the path length have been determined. If the 496.5 nm argon-ion laser line is used for the absorption wavelength and the 501.7 nm line as the transmission wavelength, then the initial intensity ratio is (with the notation of equation (22)),

$$I_a^o/I_b^o = I_{496.5}^o/I_{501.7}^o = 2.40 \qquad (25)$$

for this laser. The path length for the experimental device to measure NO_2 in the atmosphere was selected based on a detection goal of about 0.01 to 0.02 ppm. The minimum detectable change in the transmitted intensity ratio was estimated to be 5 percent. Using these criteria and the NO_2 absorption coefficients, equation (22) can be used to predict a needed path length of between 4525 m (0.02 ppm) and 9050 m (0.01 ppm). A suitable office building was found at a location 3540 m from the laser location, resulting in a total path length from the laser to the reflector on the building and back to the receiving unit of 7080 m. This corresponds to a minimum detectable NO_2 concentration of 0.0128 ppm for the 5 percent ratio change.

Now equation (22) can be rewritten using the argon-ion laser wavelength 496.5 nm for the absorption line and 501.7 nm for the transmission line.

$$c = 1/((\sigma_{496.5} - \sigma_{501.7})R)(\log_e(I^{\circ}_{496.5}/I^{\circ}_{501.7}) \qquad (26)$$

$$- \log_e(I_{496.5}/I_{501.7}) - (\beta_{496.5} - \beta_{501.7})R$$

$$- (\delta_{496.5} - \delta_{501.7})R - (\gamma_{496.5} - \gamma_{501.7}))$$

which can be put in terms of the NO_2 concentration c, the measured intensity ratio $(I_{496.5}/I_{501.7})$, and constants, by using the values presented in this paper. The attenuation coefficients (scattering)

are given in Table 1, the absorption coefficients are presented in Table 4, and the path length and initial intensity ratio are given in this chapter. These values are repeated below:

$$(\sigma_{496.5} - \sigma_{501.7}) = 0.567 \times 10^{-3} (\text{ppm})^{-1} \text{m}^{-1}$$

$$R = 7080 \text{ m}$$

$$(I^{o}_{496.5}/I^{o}_{501.7}) = 2.40$$

$$(\beta_{496.5} - \beta_{501.7}) = 0.74 \times 10^{-6} \text{m}^{-1}$$

$$(\delta_{496.5} - \delta_{501.7}) = 0.1035 \times 10^{-4} \text{m}^{-1} \text{ at V = 4 km}$$

$$0.5803 \times 10^{-5} \text{m}^{-1} \text{ at V = 10 km}$$

$$0.451 \times 10^{-5} \text{m}^{-1} \text{ at V = 15 km}$$

$$(\gamma_{496.5} - \gamma_{501.7}) = 0.596 \times 10^{-2}$$

When these values are substituted into equation (26) the following equation results,

$$c = y - 0.249 \log_e (I_{496.5}/I_{501.7}) \qquad (27)$$

where

$y = 0.197$ at $V = 4$ km

$y = 0.205$ at $V = 10$ km

$y = 0.207$ at $V = 15$ km

$y = 0.218$ if all scattering coefficients are zero and only absorption coefficients are considered.

Equation (27) is plotted in Figure 6 for the three different visibilities corresponding to three different values for the Mie attenuation coefficient. For the purpose of comparison, the case is also shown where only attenuation by absorption is considered with no scattering effects.

Interferences

One assumption which has been made but not properly justified in developing the absorption theory in this paper is that NO_2 will be the only gas absorbing the argon-ion laser lines. It is difficult to justify this assumption completely because of the lack of complete and organized spectrophotometric data on every substance which occurs in the atmosphere, either naturally or from man-made sources. From the data available, it appears that there are no appreciable interferences (amounts of absorption) by atmospheric constituents other than NO_2 for the two argon-ion laser lines of interest - the 496.5 and the 501.7 nm lines.

Leighton[31] gives the most complete list available of atmospheric gases and their radiation absorption characteristics in the region 300 to 700 nm. This list is reproduced in Table 6 along with comments on the wavelengths and strength of absorption relative to the argon-ion

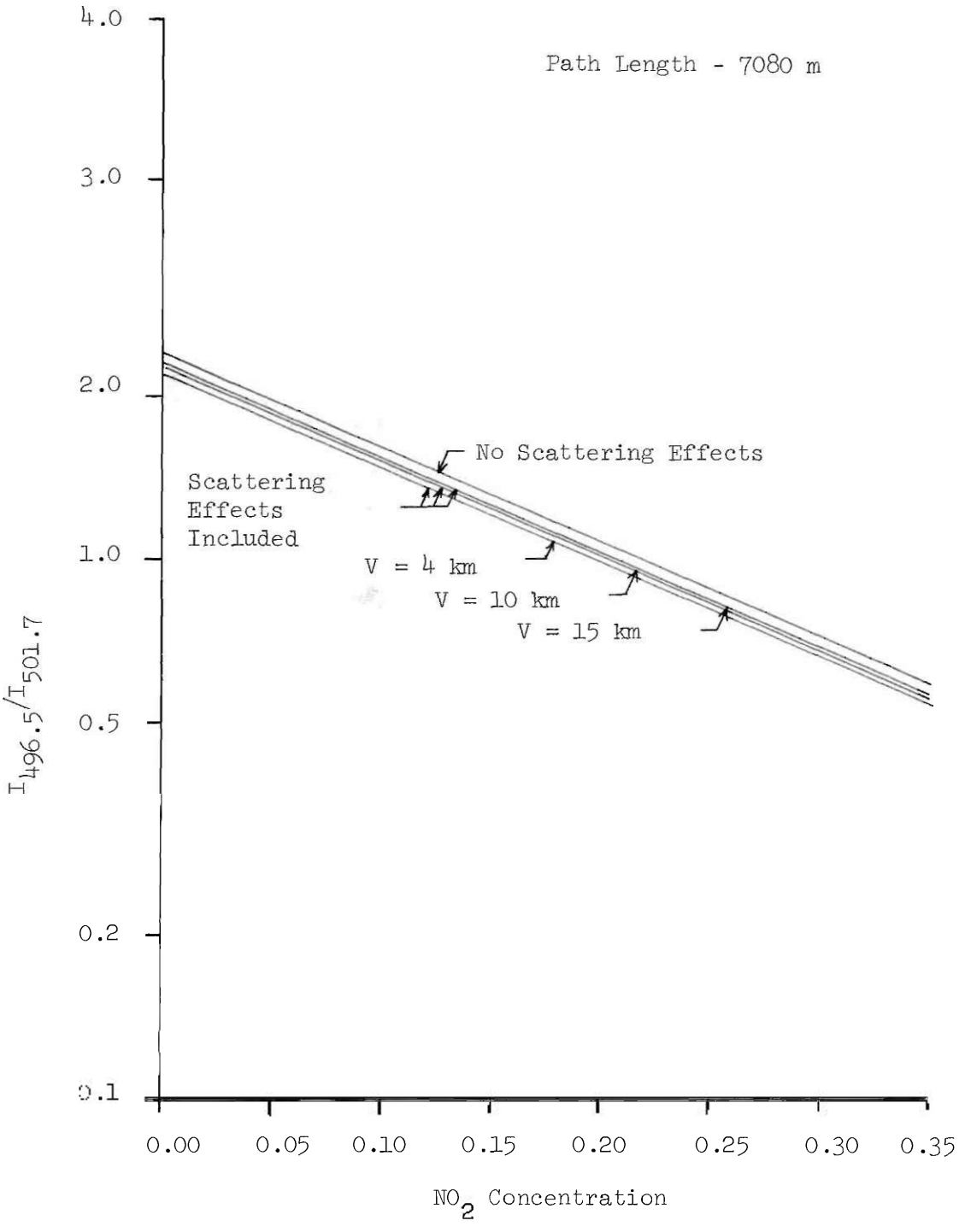

Figure 6. Ratio of Transmitted Intensity of Two Argon-ion Laser Wavelengths as a Function of NO_2 Concentration.

Table 6. Absorption Properties of Atmospheric Constituents in the Region 300 to 700 nm. (After Leighton[31])

Atmospheric Constituent	Absorption Region λ, nm	Approximate Average Strength base 10; $mmHg^{-1}cm^{-1}$
Nonabsorbers		
Nitrogen		
Water		
Carbon monoxide		
Nitric oxide		
Sulfur trioxide and sulfuric acid		
Hydrocarbons		
Alcohols		
Organic acids		
Absorbers		
Nitrogen dioxide	300-700	
	480	0.49×10^{-2}
	490	0.43×10^{-2}
	500	0.37×10^{-2}
	525	0.27×10^{-2}
Ozone (Chappuis bands)	450-700	
	475	0.6×10^{-5}
	500	1.6×10^{-5}
	525	2.8×10^{-5}
Oxygen	687-692	4×10^{-10}
	759-766	10^{-9}
Sulfur dioxide	<395	
Nitric acid	<330	
Ethyl nitrate	<330	
Nitrous acid	<385	

Table 6. (Continued).

Atmospheric Constituent	Absorption Region λ, nm	Approximate Average Strength base 10; $mmHg^{-1}\,cm^{-1}$
Absorbers (Continued)		
Methyl, ethyl, amyl nitrates	300-400	
Ethyl nitrite	<410	
Nitroethane	<350	
Aldehydes and ketones (most, except for biacetyl) (biacetyl)	<372 <470	0.3×10^{-4}
Peroxides	<370	
PAN	<310	

wavelengths of interest. In addition to those substances listed, Leighton mentions other possible atmospheric absorbers for which no absorption coefficients exist; these include free radicals, unstable molecules such as nitroxyl and nitrogen trioxide, organic compounds such as ozonides, epoxides, dienes, nitroso compounds, peroxidic compounds, benzpyrene, and other related compounds.

The conclusion drawn from the data presented in Table 6 is that the only probable interferences with the NO_2 absorption of the argon-ion lines of interest is that of ozone which has a coefficient 1/230 as strong as NO_2 at 500 nm. But the concentration of ozone in urban atmospheres is about the same order of magnitude as NO_2 concentration (Continuous Air Monitoring Program monthly average:[32] NO_2 0.037 ppm, oxidants 0.028 ppm). So ozone interferences should be negligible in the troposphere.

Experimental Apparatus

An experiment designed to apply the laboratory work resulting in equation (27) was constructed as described below, and an improved system which is presently under construction will be described later in this paper.

The laser and receiving optics for doing the real atmosphere studies were located in the Physics Building on the campus of Georgia Institute of Technology. The site is about 2.6 km (1.6 miles) from the center of downtown Atlanta. The laser and the receiving optics were situated in front of a window on the fifth floor of the Physics Building. A corner cube reflector was mounted 3.54 km (2.2 miles)

almost due north (away from the downtown area) on top of an eight story office building (Sheffield Building). As can be seen from Figure 7, this light path was roughly parallel to the major downtown expressway and varied from 0.6 km (0.4 miles) away from it to passing directly overhead, at an average height above ground of 30 meters. According to measurements taken by the Fulton County Health Department, the area around Georgia Institute of Technology had the highest mean NO_2 concentration of the sampling stations in Atlanta in 1971 with a mean 24 hour average of 0.108 ppm based on a small number of samples.

A block diagram of the apparatus used in the real atmosphere tests is presented in Figure 8. The laser and optics were mounted on a stable platform built from cement blocks and two sheets of plywood. The light source used was a TRW Instruments Model 91B pulsed argon-ion laser with output characteristics as presented in Table 7. The output optics used in addition to the laser were two 45°-45°-90° prisms to reverse the beam direction, and a five power telescope for enlarging the beam to reduce divergence and for focusing the beam. The divergence of the beam coming directly from the laser is 5.5 milliradians but this is reduced by the ratio of the focal lengths of the lenses which is the same as the power of the telescope. Thus, after passing through the five power telescope, the divergance is 1.1 milliradians if the telescope is focused for an infinite distance. This would result in a beam diameter of 3.9 m at the corner cube reflecter. If the beam were focused onto the corner cube reflector, the diffraction limited spot assuming a uniform light distribution at the telescope would be 0.22 m in diameter. Due

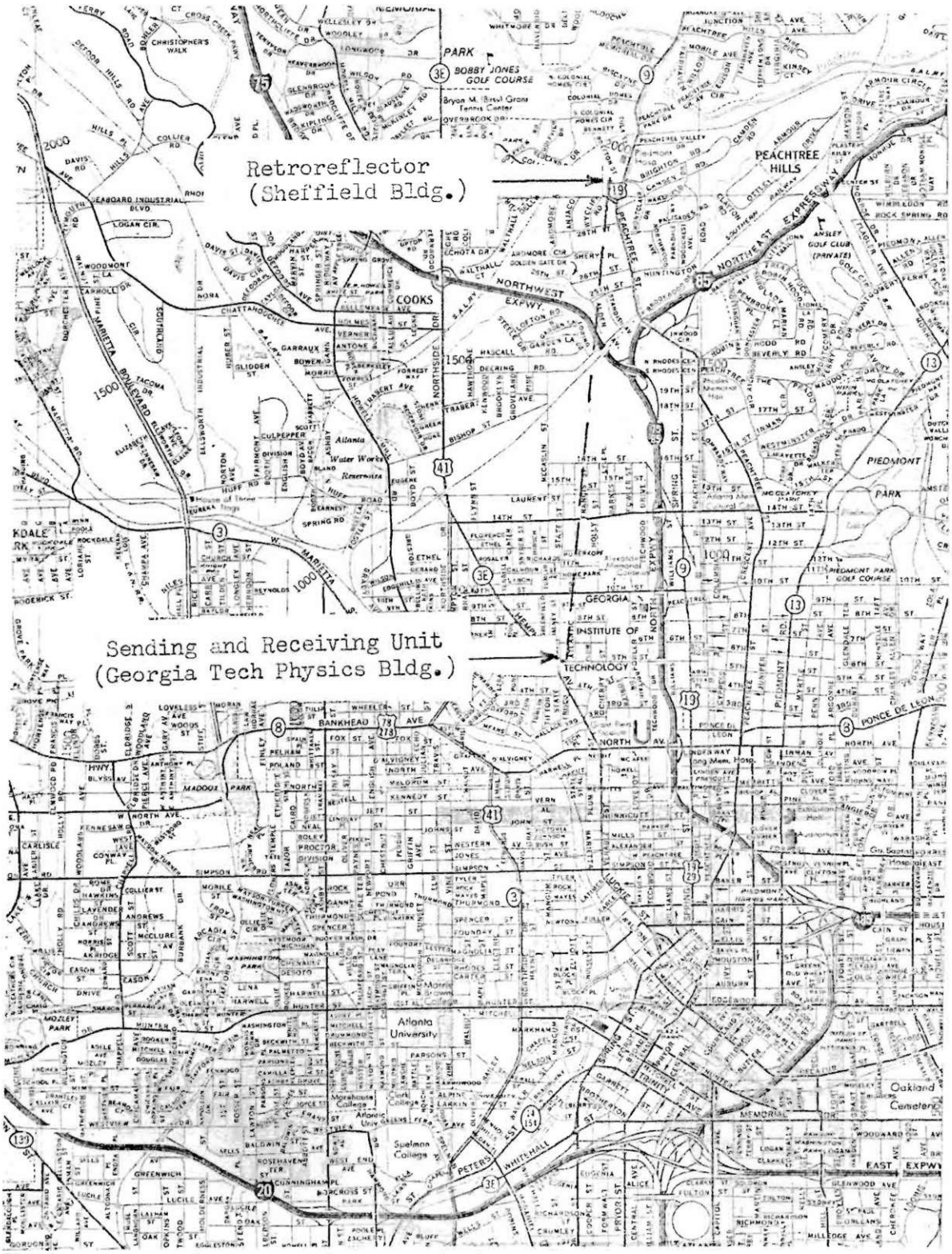

Figure 7. Map of Laser Beam Path.

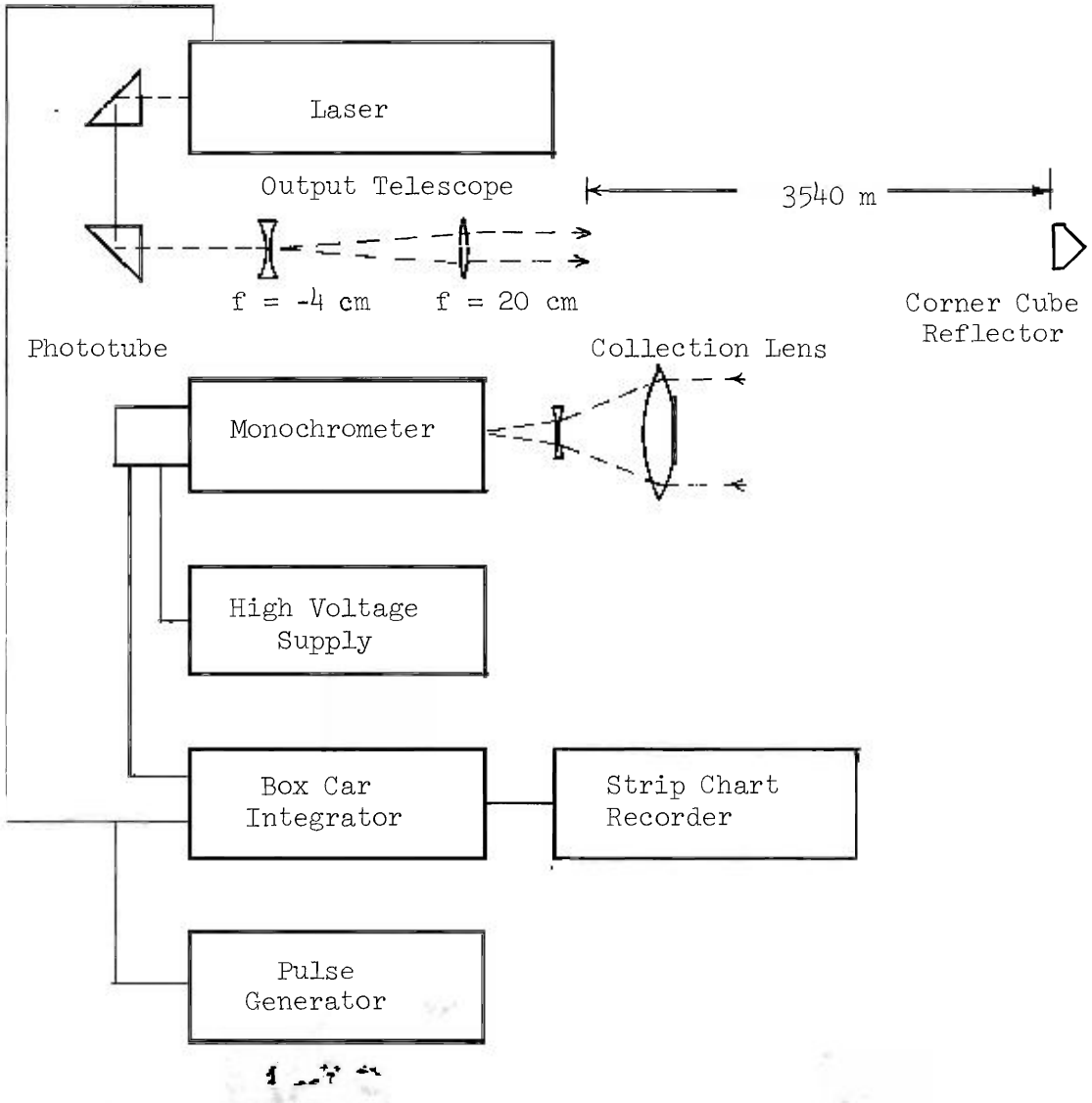

Figure 8. Block Diagram of NO_2 Measurement System.

Table 7. Output Characteristics of the Argon-ion Laser. (For multimode operation)

Peak Power, multicolor	3.0 watts (W)
Average Power (55 Hz)	
multicolor	6.6 milliwatts (mW)
Specific wavelengths:	
λ = 476.5 nm	0.69 mW
λ = 488.0 nm	2.18 mW
λ = 496.5 nm	0.62 mW
λ = 501.7	0.26 mW
λ = 514.5 nm	2.85 mW
Pulsewidth	40 μsec
Pulse Rate (external trigger)	55 Hz
Beam Divergence (whole angle)	5.5 milliradians

to the mode pattern in the beam the actual spot diameter is between 0.22 m and 3.9 m, assuming no spreading due to atmospheric effects.

Part of the beam was intercepted at a distance of 3540 m by a 3.5 cm diameter cylindrical glass corner cube reflector mounted in a protective housing. A corner cube reflector has the property that it accurately reflects light parallel to the incident beam, if the incident light is approximately ($\pm 20^{\circ}$) perpendicular to the front face of the prism. The properties of corner cube reflectors are well presented by Eckhardt[33], except for diffraction effects which are discussed in Appendix C of this paper. As shown in the appendix, the light returned by the corner cube reflector comes in six overlapping spots 36 cm in diameter and centered at the corners of a hexagon 4 cm across. This pattern is centered on the output laser beam axis.

Part of the return beam was intercepted by the 10.2 cm collecting lens which was used with a negative lens to focus the light through a pinhole and into the Jarrell-Ash Model 82-410 0.25 meter monochrometer. The negative lens was used so that the full diameter of the large collecting lens could be used without exceeding the aperture stop of the monochrometer (f/3.6). The geometry of the return beam and the collection system is shown in Figure 9. Various sizes of entrance pinholes were used from 25 μm to 1000 μm. For the diurnal variation work reported on later, the 1000 μm (1 mm) entrance pinhole was used.

The output of the monochrometer was detected by a RCA Model

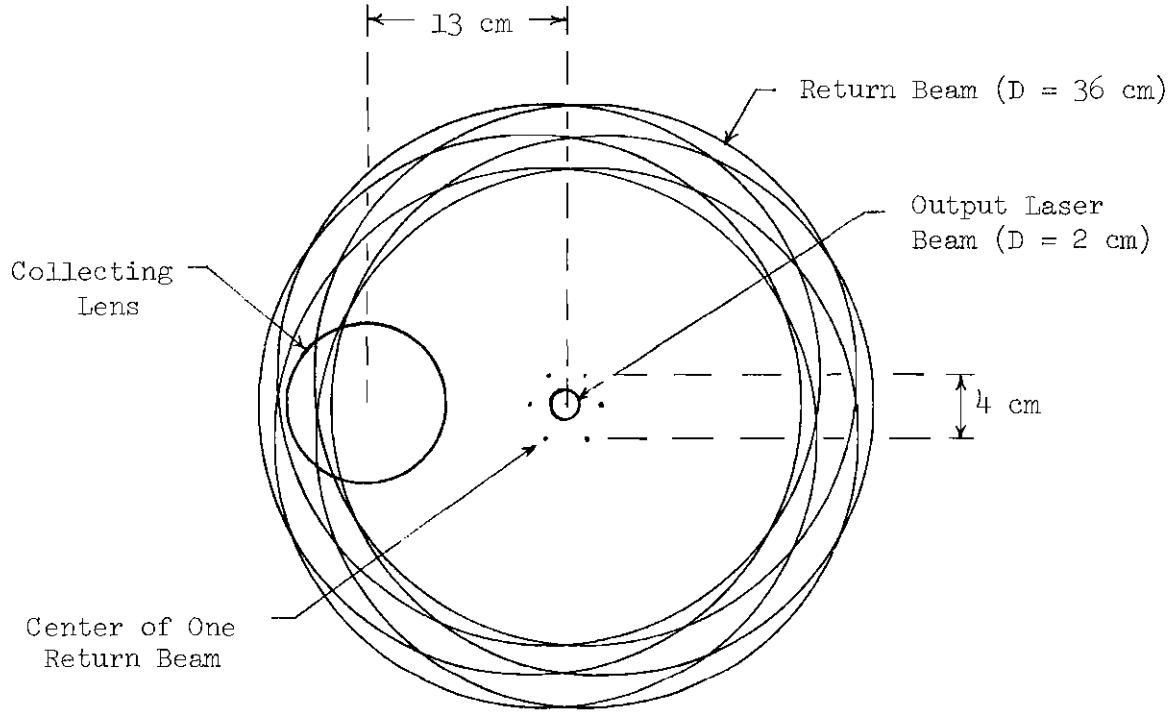

Figure 9. Return Beam Collection Optics.

1P28 multiplier phototube which was supplied voltage by a Harrison Model 6515A DC power supply. As was explained in Chapter III, the average phototube current was restricted to be less than 0.022 μA when used with the argon-ion laser to assure that the peak current remained in the linear region of the phototube (less than 10.0 μA).

The output of the phototube served as an input for a Princeton Applied Research Model CW-1 box car integrator which served as a gate and an amplifier for the phototube signal. The laser was pulsed at approximately 55 Hz with a Techtronix Type 114 pulse generator and the trigger pulse was also sent to the box car integrator to open the input gate for 65 μsec. This allowed the box car integrator to monitor the 40 μsec pulse of the laser after the 24 μsec delay for travel time of the laser beam, but to discriminate against ambient light contributions by being "turned off" the rest of the time. Because the box car integrator gate was closed 99.64 percent of the time, the signal to noise ratio was improved by a factor of 280 over a non-gated input. The combination of the entrance pinhole on the monochrometer and the gate in the box car integrator reduced the noise due to ambient light conditions to an unmeasurable quantity relative to the laser signal even during the brightest period of a clear day. The output of the box car integrator was directly proportional to the input signal, in this case, the intensity of the transmitted laser line, but was electronically averaged with a variable time constant. Most of the work was done with a time constant of 1 msec. This output was then recorded on a Keithley Model 370

recorder.

Results of Real Atmosphere Tests

The procedure used to measure the relative intensities of the argon-ion laser lines was to scan the monochrometer across all five of the laser wavelengths (or just the two of interest) at a rate of 5 nm per minute. The time constant of 1 msec was used to smooth the variations in the return intensity. This allowed average values for the 496.5 nm line and 501.7 nm line to be compared, although they were not measured at exactly the same time.

Two spectra of the laser lines transmitted through the atmosphere are presented in Figures 10 and 11, both with time constants of 1 msec. Figure 10 displays the spectrum obtained with an entrance pinhole of 25 μm and an exit slit of 100 μm resulting in a resolution of 0.5 nm. Figure 11 is a much lower resolution spectrum obtained by replacing the 25 μm pinhole with a 1000 μm pinhole. Each of these were taken during sunny days but it can be seen from the figures that the background noise was zero, due to the gate operation of the box car integrator. It is clear from Figure 11 that due to refractive index fluctuations, the transmitted line intensities do vary appreciably even with the time constant in the circuit. This rapid variation prevents good reproducibility of the line intensities and is the limiting factor in the accuracy of the experiment as it has been described.

The largest source of NO_2 in the urban environment is the automobile, and for that reason NO_2 concentrations can be expected to

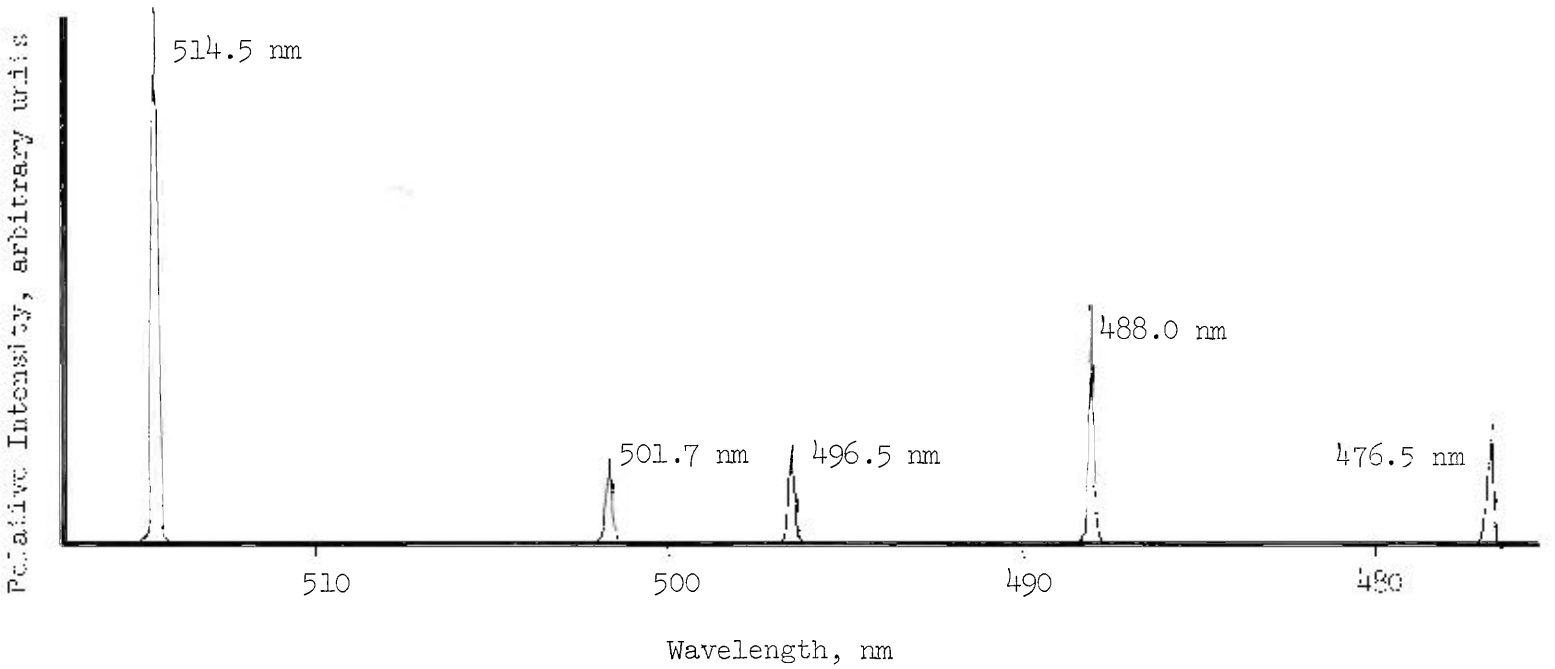

Figure 10. Spectrum of Transmitted Argon-ion Laser Lines with 25 μm Entrance Pinhole.

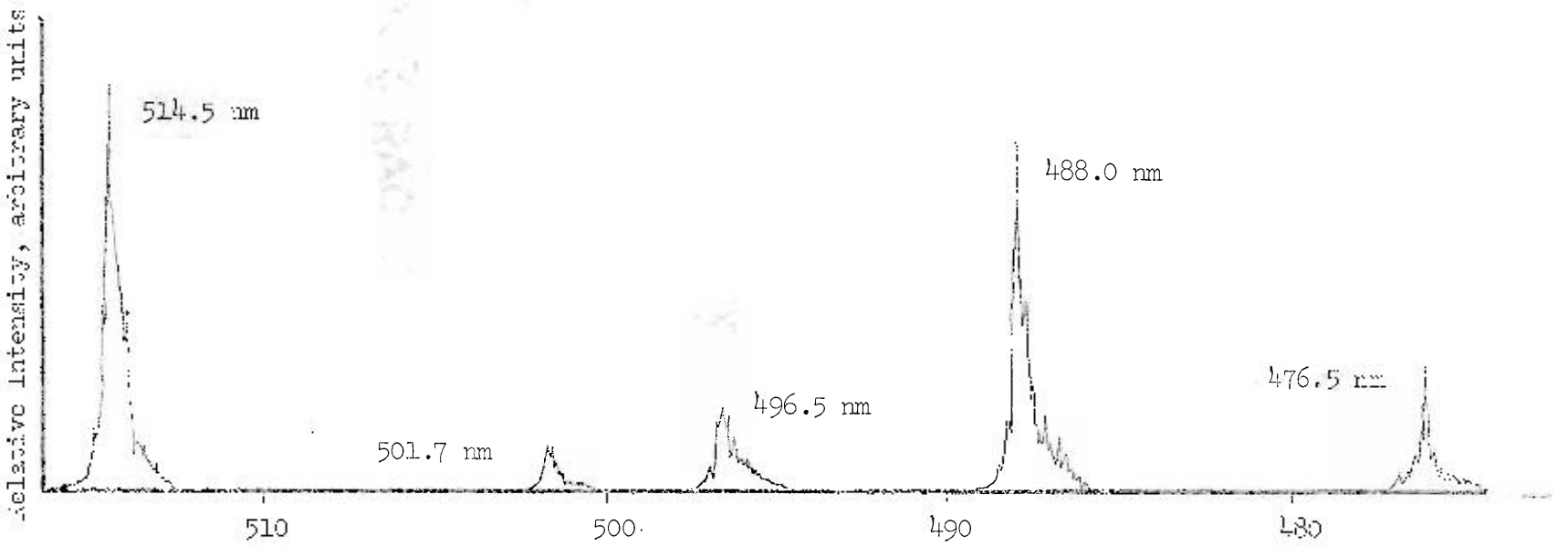

Figure 11. Spectrum of Transmitted Argon-ion Laser Lines with 1 mm Entrance Pinhole.

be correlated to traffic flow and show a similar diurnal variation. Peak concentrations usually occur from one-half to one and one-half hours after peak traffic flow[1], the delay due to the time required for photochemical conversion of the emitted NO into NO_2. The intensity ratios and resulting concentrations for a 12 hour period are plotted in Figure 12 for a series of spectra like those shown in Figure 11 (with the 1 mm pinhole). The data were taken on October 27, 1972, on a day that was sunny and clear except for some haze. The data points presented in Figure 12 are averages of three readings - the reading actually taken at the time indicated and the two readings taken before and after the central one. Even with this smoothing there was some randomness to the points but the diurnal variation can be seen in Figure 12. As previously mentioned, the location chosen was close to downtown Atlanta and peak traffic flow on the nearby expressway and streets occurs at 8:00 to 9:30 am, 12:00 to 1:00 pm, and 4:30 to 5:30 pm. The maximum NO_2 concentrations recorded followed these traffic peaks except for an unexplained peak at 3:15 pm. This diurnal variation is compared with measurements taken by other workers[1,32] in Figure 13. The data given by Ludwig, Bartle, and Griggs[32] represent two year averages of hourly measurements for six cities, while the data presented by the EPA[1] represents one days measurement of NO_2 concentration in Los Angeles in which afternoon ventilation prevented a buildup of pollutants. The concentration recorded using this experimental apparatus was more variable than the others reported, but this would be characteristic of instantaneous

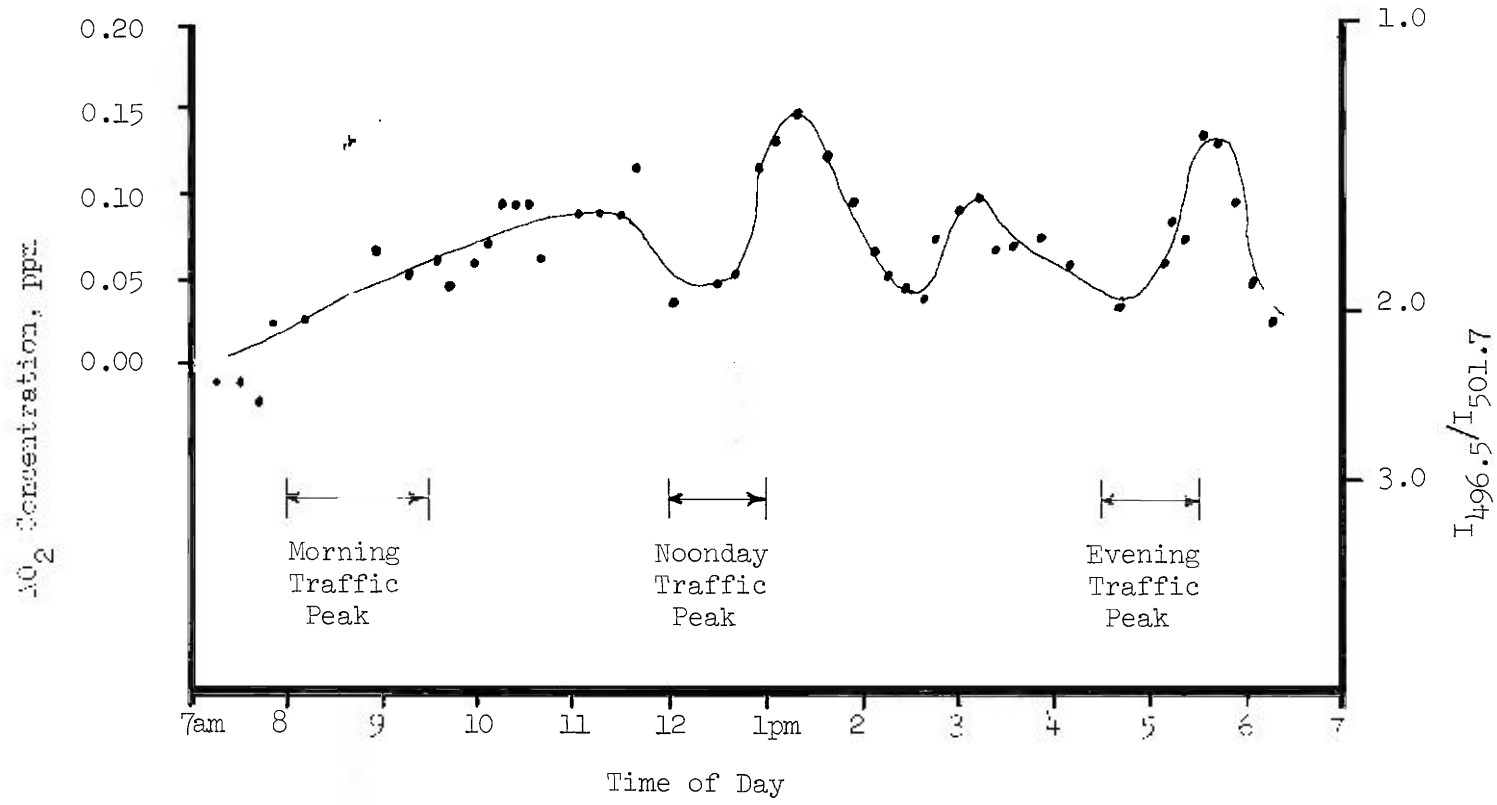

Figure 12. Measurement of Diurnal Variation of NO_2 Concentration.

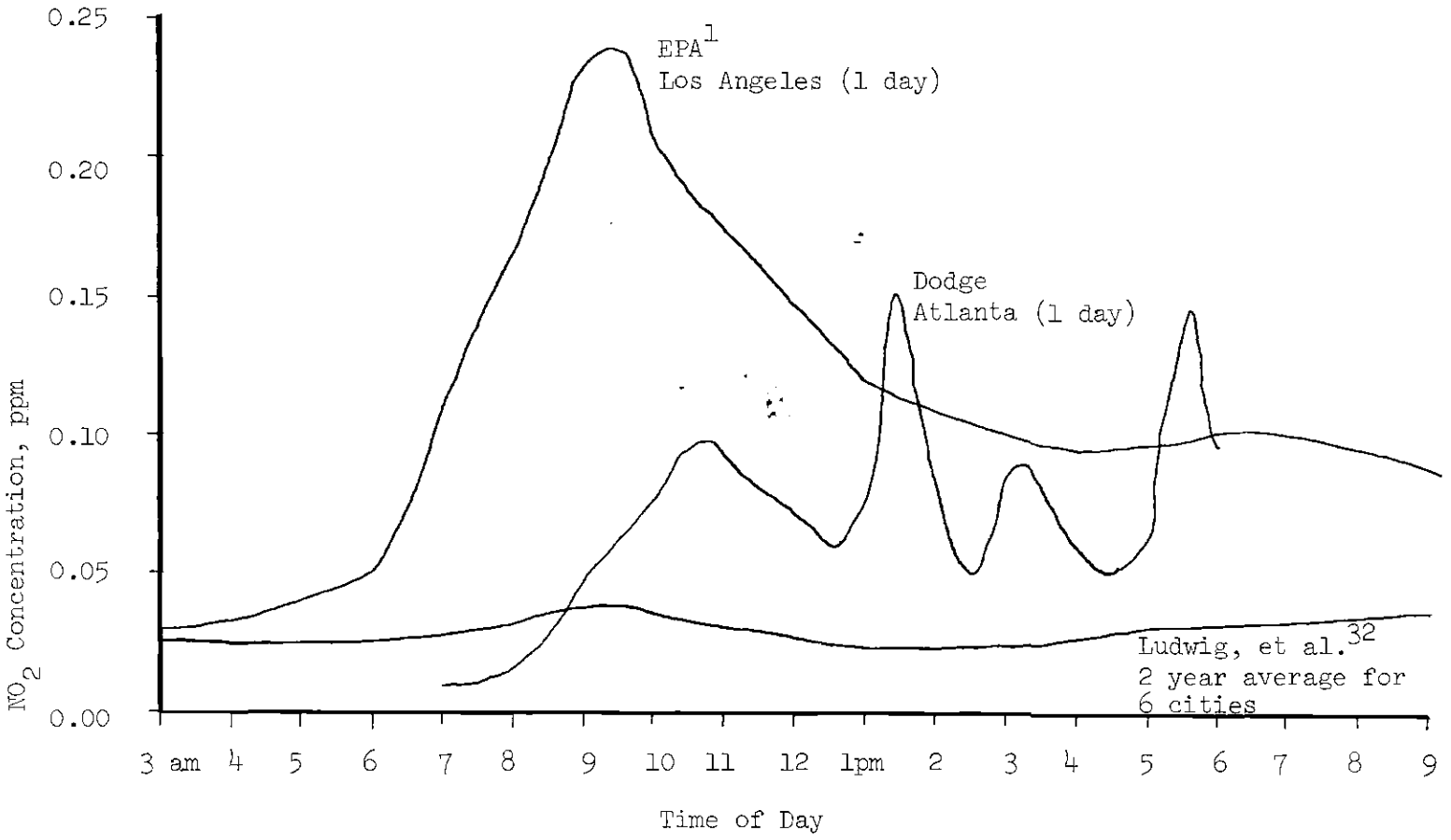

Figure 13. Comparison of Diurnal Variation of NO_2 Concentration.

sampling as opposed to hourly averaging.[32]

While the results obtained using this experimental apparatus were reasonable in that diurnal variations could be observed, they also showed that a more accurate method of obtaining intensity ratios was needed in which the intensities were measured simultaneously.

Simultaneous Measurement Technique

With some changes in the receiving optics and electronics, the apparatus previously described can be used to simultaneously and continuously measure and compare the two argon-ion laser line intensities of interest. At the present time this project is under construction.

A block diagram of the proposed system is shown in Figure 14. The output system and reflector are the same as described earlier in this chapter. Again a large collection lens is used to gather the reflected light which is focused into the Jarrell-Ash monochrometer as before, or through an alternate dispersive system made from Fresnel lenses and a holographic grating. A prototype of this second system has been constructed and operates as follows. First the light is focused onto a pinhole and then the diverging light is made parallel again by a large (10.2 x 12.7 cm) Fresnel lens. The parallel light is then dispersed by a holographic sine grating and focused by another Fresnel lens identical to the first one. Both Fresnel lenses and the sine grating are all the same size and can be mounted together as a single unit. The holographic sine grating was made with facilities in the Physics Department. The sine grating technique offers a less

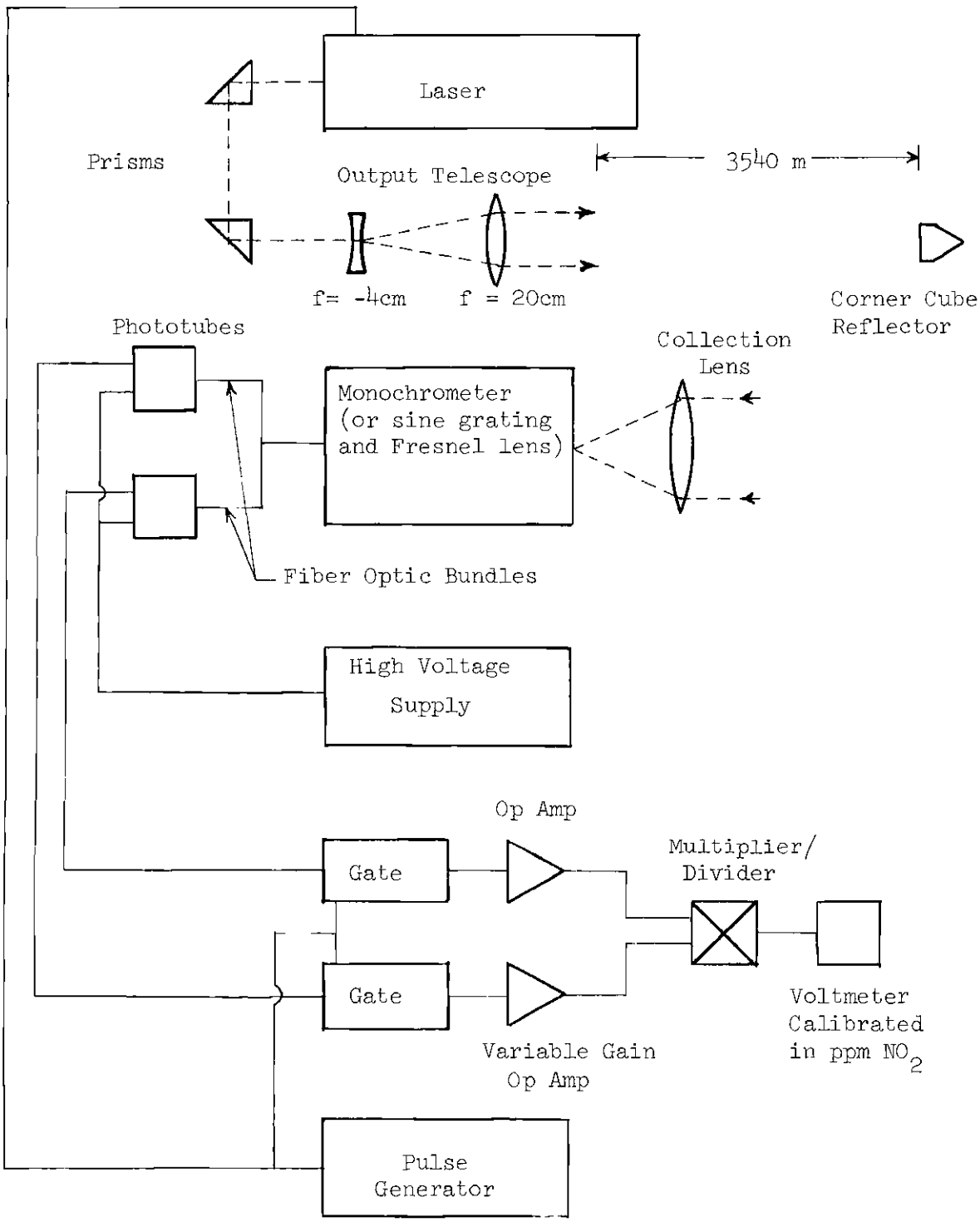

Figure 14. Apparatus for Simultaneous Intensity Measurements.

expensive dispersing system with a wider aperture stop than the monochrometer.

In the output focal plane of the holographic grating system, the 496.5 and 501.7 nm lines are 0.328 mm apart for the particular grating used (14^{o} at 633 nm), and for the monochrometer used they are 1.57 mm apart. The two beams are further separated at the output focal plane by the use of a fiber optic bundle 3 mm in diameter. This bundle terminates at one end in the output focal plane of the dispersing system, and the other end is split into two bundles each of which conducts the light incident on one-half of the other end of the bundle. Thus the separated bundles can be terminated at identical phototubes and the two line intensities can be measured simultaneously.

The output of the phototubes is fed to a pair of synchronous gates which serve to permit passage of the phototube current only while the laser signal is present. The gating signal from the Tektronix Type 114 pulse generator is sent simultaneously to the laser and to the two gates. The gates then stay open for 65 μsec which allows time to measure the 40 μsec pulse after its return from the reflector. The outputs of the phototubes, after passing through the gates, are amplified by operational amplifiers and the two signals are compared by an analogue multiplier/divider. The output of the multiplier/divider, when set in the divide mode, is proportional to the ratio of the input signals. Thus, a voltmeter connected to the output of the multiplier/divider can be calibrated with a logarithmic scale which

indicates the NO_2 concentration. The relationship between the laser line intensity ratio and the concentration is given by equation (27) with y = 0.205,

$$c = 0.205 - 0.249 \times \log_e(I_{496.5}/I_{501.7}). \qquad (28)$$

The zero calibration can be made by sending a portion of the output beam directly into the collecting lens and then adjusting the variable gain operational amplifier to give a zero reading on the concentration scale.

CHAPTER V

CONCLUSIONS

In conducting this investigation, a relatively high resolution (0.5 nm) spectrum of nitrogen dioxide absorption in the visible region has been measured and presented in Figure 3. The absorption coefficients of nitrogen dioxide for the output wavelengths of a mercury lamp and an argon-ion laser have been measured and are reported in Tables 3 and 4. Beer's Law was obeyed over the regions observed as shown in Figures 4 and 5.

Some theoretical analyses of remote laser detection schemes have not adequately considered the large rapid fluctuations in intensity of transmitted laser beams due to atmospheric refractive index fluctuations. Simultaneous measurement of two wavelengths with different absorption coefficients for the gas of interest should enable one to distinguish between the attenuation due to absorption from that due to refractive index scattering. In comparing the intensity attenuation for two wavelengths, the variation of the absorption coefficient with wavelength must be large compared to the variation of the scattering attenuation coefficients (for the several scattering processes) with wavelength. This criterion is satisfied for nitrogen dioxide at various places in the region 400 to 550 nm. Also, the absorption coefficient multiplied by the gas concentration for the gas of interest must be large compared to similar coefficient times concentration

product for other atmospheric constituents. This criterion is satisfied for nitrogen dioxide in the troposphere for the two argon-ion lines (496.5 and 501.7 nm) used in this study.

The use of electronic gates in the signal receiving apparatus allows the use of a low average power, inexpensive, non-hazardous, pulsed laser which has a signal to noise ratio equivalent to a continuous wave (cw) laser system operating at the peak power of the pulsed laser. The use of gates improves the signal to noise ratio over the nongated input by approximately the inverse of the duty cycle of the pulsed laser.

Preliminary tests have shown that the light absorption detection method is capable of monitoring the diurnal variation of nitrogen dioxide. No final conclusions can be made at this time about the minimum sensitivity of this detection scheme until the simultaneous intensity measurement method has been evaluated.

APPENDIX A

THE NITROGEN DIOXIDE PRESSURE IN THE WHITE CELL

Because the amount of absorption of radiation by NO_2 is proportional to the number of molecules present, it is necessary to calculate the dissociation occurring when the N_2O_4 and NO_2 mixture in V_a is bled into the White cell. The dissociation of N_2O_4 into NO_2 has been studied in detail by Verhock and Daniels.[34] They give the equations for calculating the dissociation factors at pressures of 0.15 to 1.0 atm and temperatures of 25°C, 35°C, and 45°C. In order to use these equations it was necessary to extrapolate values for 22.8°C and to make a large extrapolation in pressure to 10^{-4} atm. Dixon[16] found the equations given by Verhock and Daniels to be valid at 0.007 atm, and the equations predict almost complete dissociation at 10^{-4} atm which is in agreement with the observed properties of NO_2 when diluted in the atmosphere to a low partial pressure. The equations predict 99.8 percent dissociation at the 124 μmHg (0.164×10^{-3} atm) partial pressure of NO_2 which existed in the White cell, and 13.4 percent dissociation at the 1.08 atm pressure in V_a. These calculations are given below, using the notation of Verhock and Daniels with some additions.

Define the degree of dissociation α by

$$\alpha = (P - p^{\circ}_{N_2O_4})/p^{\circ}_{N_2O_4}$$

where P is the measured pressure (NO_2 and N_2O_4), and $p^o_{N_2O_4}$ is the ideal pressure if no dissociation occurred. So $\alpha = 0$ implies no dissociation and $\alpha = 1$ means complete dissociation of N_2O_4 into NO_2. Define the dissociation constant $K_{N_2O_4}$ as

$$K_{N_2O_4} = (4\alpha^2 P)/(1 - \alpha^2)$$

The equations given by Verhock and Daniels are for $K_{N_2O_4}$ as a function of temperature and molar concentration. Since the degree of dissociation α is needed as a function of temperature and pressure for this experiment, the above equation for $K_{N_2O_4}$ was solved for α,

$$\alpha = \sqrt{K_{N_2O_4}/(4P + K_{N_2O_4})}$$

and the equations for $K_{N_2O_4}$ at several temperatures are given as,

$$K = 0.1426 - 0.7588 \times C^o_{N_2O_4} \text{ at } 25^oC$$

$$K = 0.3183 - 1.591 \times C^o_{N_2O_4} \text{ at } 35^oC$$

$$K = 0.6706 - 3.382 \times C^o_{N_2O_4} \text{ at } 45^oC$$

where K is the same as $K_{N_2O_4}$ and $C^o_{N_2O_4}$ is the concentration in g.mole/liter of N_2O_4 that would exist if there were no dissociation. An

extrapolation of the constant and multiplier terms in the above equations to the desired temperature of 22.8°C gives,

$$K = 0.118 - 0.59 \times C^{o}_{N_2O_4} \text{ at } 22.8^{o}C.$$

In calculating the dissociation in V_a and in the White cell it was necessary to use an iterative process, because not all the needed parameters were known. Thus, to calculate α for V_a it was first necessary to estimate some value for $C^{o}_{N_2O_4}$ which was used to calculate α which was in turn used to improve the estimate of $C^{o}_{N_2O_4}$. This process quickly converged to a value for α good to three significant figures.

To calculate α for V_a assume for a first approximation that $\alpha = 0.16$ which is a reasonable value from the literature. Then,

$$C^{o}_{N_2O_4} = n^{o}_{N_2O_4}/V = p^{o}_{N_2O_4}/RT$$

from the definition of $C^{o}_{N_2O_4}$ and the ideal gas law, where $n^{o}_{N_2O_4}$ is the number of moles of N_2O_4 present if no dissociation occurs, V is the value, R is the gas constant, and T is the temperature. The vapor pressure of N_2O_4 and NO_2 at 22.8°C is[28] 1.081 atm (P = 1.081 atm) and the assumed dissociation is 0.16, which gives $p^{o}_{N_2O_4} = 0.9317$ atm and $C^{o}_{N_2O_4} = 0.0384$ g.mole/liter. Then K = 0.0953 atm and $\alpha = 0.1343$. Using this value of α, $C^{o}_{N_2O_4}$ is recalculated as 0.03925 g.mole/liter and K = 0.0949 atm which gives $\alpha = 0.1342$. This is in close agreement with the above figure for α and is taken as the correct value for

the degree of dissociation for V_a.

A similar calculation is made for α for the N_2O_4 and NO_2 mixture at the reduced pressure in the White cell. For the first iteration it was assumed that $\alpha = 1.00$ (totally dissociated) since the mixture was so dilute. The "measured" pressure P was assumed to be 125 μmHg (0.164×10^{-3}atm) which would be the approximate resultant pressure if the N_2O_4 which existed in V_a were completely dissociated in the White Cell. The value for $C^{\circ}_{N_2O_4}$ was estimated from $C^{\circ}_{N_2O_4}$ for V_a but was reduced by the ratio of the volume of the White cell to V_a.

$$C^{\circ}_{N_2O_4} = (11.2 \text{ ml}/1.31 \times 10^{5} \text{ ml}) \times 0.03925 \text{ g.mole/liter}$$

$$C^{\circ}_{N_2O_4} = 0.335 \times 10^{-5} \text{ g.mole/liter}$$

This gives a value for K of 0.118 atm and

$$\alpha = K/(4P + K)$$

$$\alpha = 0.118/(0.000656 + 0.118)$$

$$\alpha = 1/(0.00556 + 1)$$

This can be evaluated using the approximation,

$$(1 + x)^{-\frac{1}{2}} = 1 - (1/2)x \qquad x^2 \ll 1.$$

Using this approximation,

$$\alpha \cong 1 - (1/2)(0.00556) = 0.9982.$$

This is very close to complete dissociation and for simplicity it is assumed $\alpha = 1.00$ in the White cell.

To calculate the pressure of NO_2 in the White cell, the known partial pressures of N_2O_4 and NO_2 in V_a are used along with the ratio of the volume of V_a to the White cell. As the NO_2 leaves V_a and goes into the White cell, its partial pressure is reduced by the ratio of the volumes. But since the N_2O_4 dissociates into two molecules of NO_2, the N_2O_4 partial pressure is reduced by only one-half of the ratio of the volumes. Thus the pressure of NO_2 in the White cell is given by,

$$P_{wc} = (p^{V_a}_{N_2O_4} \times (V_a/V_{wc}) \times 2) +$$

$$+ (p^{V_a}_{NO_2} \times (V_a/V_{wc}))$$

$$P_{wc} = (0.824 \text{ atm} \times 0.855\text{x}10^{-4} \times 2) + (0.256 \text{ atm} \times 0.855\text{x}10^{-4})$$

$$P_{wc} = 1.629 \times 10^{-4} \text{ atm} = 124 \text{ } \mu\text{mHg}$$

This is very close to the original estimate of P = 125 μmHg so it is not necessary to re-evaluate α and P. Thus, the resultant NO_2 pressure in the White cell when one unit of N_2O_4 and NO_2 mixture in V_a is bled into the White cell is 124 μmHg, and this is almost entirely NO_2 with very little N_2O_4 present.

APPENDIX B

SPECTRAL LINE BROADENING

The broadening of spectral lines about the theoretical wavelength (or frequency) for a given transition is due to several factors:

(1) the finite lifetime of the excited state gives rise to an uncertainty in the excited energy as shown by the uncertainty principle, and this results in a spread of allowed frequencies for a transition;

(2) Doppler shifts in frequency due to relative thermal velocities of molecules;

(3) perturbations due to collisions of the absorbing or emitting molecule with other molecules.

An order of magnitude estimate is made below for each of these line broadening mechanisms as they effect the line width of the NO_2 sample in the White cell.

"Natural line broadening" due to the uncertainty relation can be demonstrated from the uncertainty relation,[35]

$$\Delta E \; \Delta t \geq h/2\pi$$

where ΔE is the energy uncertainty, Δt is the lifetime of the excited state, and h is Planck's constant. Since $E = h\nu$ for photons, the

uncertainty in frequency $\Delta\nu$ is related to the uncertainty in energy by $\Delta E = h\Delta\nu$ so that the uncertainty relation in terms of the frequency is

$$\Delta\nu \geq 1/(2\pi\Delta t)$$

Estimates for the lifetime of two excited states of NO_2 are given by Neuberger and Duncan[36] as $\Delta t = 2.6 \times 10^{-7}$ sec and 4.4×10^{-5} sec. The shorter the lifetime the greater the frequency uncertainty, so considering $\Delta t = 2.6 \times 10^{-7}$ sec, then $\Delta\nu \cong 0.61$ sec^{-1}. This uncertainty can be expressed in terms of wavelength by taking the differential of both sides of $\nu = c/\lambda$ to get,

$$\Delta\lambda = \Delta\nu \ (\lambda^2/c)$$

which for $\lambda \cong 500$ nm gives $\Delta\lambda \cong 0.5\ 10^{-6}$ nm. In terms of wavenumber $k = 1/\lambda = \nu/c$ the uncertainty is $\Delta k = 0.2 \times 10^{-4}$ cm^{-1}.

A second line broadening factor is due to the Doppler principle from which it follows that if a source of light of wavelength λ_o is moving in the line of sight with velocity v relative to the observer, the apparent wavelength λ measured by the observer will be[37]

$$\lambda = \lambda_o(1 + (v/c))$$

where c is the velocity of light. Since the range of relative

molecular velocities increases with temperature, so must the range of wavelengths comprising the spectral line increase. For a Maxwellian distribution of velocities, the total line width at the half maximum intensity points is given by,[37]

$$\Delta\lambda = 1.67(\lambda_o/c)\sqrt{(2kT/m)}$$

where $\Delta\lambda$ is the wavelength range, λ_o is the wavelength of the center of the line, k is Boltzmann's constant, T is the absolute temperature, and m is the mass of the atom or molecule. Note that this is independent of the pressure of the gas. For a wavelength $\lambda \cong 500$ nm, which is the region of the argon-ion laser output, the line width is on the order of $\Delta\lambda \cong 10^{-3}$ nm, or expressed in terms of the wavenumber $\Delta k = 0.04$ cm^{-1}.

The third effect contributing to line broadening is called pressure broadening which is due to perturbations of the radiating or absorbing molecule by other molecules, ions, or electrons. The amount of broadening produced depends on the pressure and on the nature of the perturbing species. An approximation of the frequency broadening for the total frequency range across the half intensity points is given by[21]

$$\Delta\nu = 1/(2\pi\tau)$$

where τ is the mean collision time. This equation is the same as the relation derived from the uncertainty principle for natural line

broadening, except that the natural lifetime Δt is replaced by the mean collision time τ. The equation is based on the assumption that τ is less than Δt and that whenever an excited molecule sustains a collision, a downward transition is induced. Hence, τ becomes the limiting factor on the lifetime of the excited state with a corresponding uncertainty in the energy and frequency. Pressure or collisional broadening is usually the dominant effect at atmospheric pressure, but it decreases linearly with pressure. The mean collision time is given by[38]

$$\tau = 1/(\sqrt{2}\ \bar{v}\ n\ \sigma_o)$$

where $\bar{v}$ is the mean velocity, n is the density of molecules, and σ_o is the scattering cross section. For the NO_2 in the White cell at a pressure of about 200 μmHg, the frequency spread is $\Delta\nu \cong 0.25 \times 10^5$ sec^{-1} which corresponds, at the argon-ion laser wavelengths, to a line width of $\Delta\lambda \cong 0.2 \times 10^{-7}$ nm, or expressed in terms of the wavenumber $\Delta k = 10^{-6}$ cm^{-1}.

Therefore, the line broadening in the experiment in the White cell was due principally to the Doppler effect and the total line width due to all the processes is about 10^{-3} nm.

APPENDIX C

DIFFRACTION EFFECTS OF CORNER CUBE REFLECTORS

Eckhardt[33] gives a complete description of the theory of corner cube reflectors except for his treatment of diffraction effects. These diffraction effects will be discussed for the type of corner cube reflector with which this author has had experience.

The corner cubes used in this experiment were made commercially from a cylinder of glass, one end of which was cut off flat while the other end was cut with three mutually orthogonal faces. The view presented on looking into the end cut off flat is similar to the view that would be given by looking at the intersection of two walls and the ceiling of a room if the walls and ceiling were covered by mirrors. In looking into the corner cube reflector, one sees the three real edges and three "apparent" edges in reflection as shown in Figure 15.

Eckhardt treats the diffraction effects of the reflector just as if the corner cube were a circular aperture with a diameter the size of the front face of the reflector. However, the edges at the intersection of the rear faces of the cube also contribute to the diffraction pattern, and the "apparent" edges act as if they contribute because the real edges act as diffracting edges for each of two reflections which each beam makes before leaving the reflector.

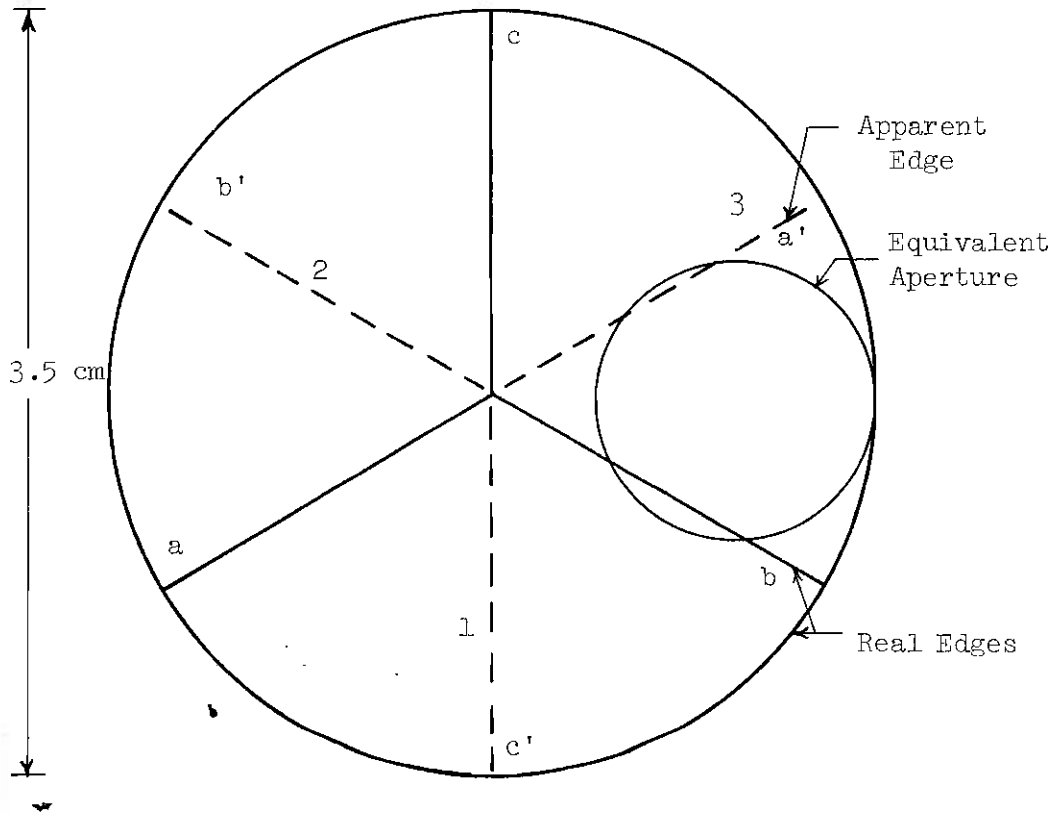

Figure 15. Front View of Corner Cube Reflector.

This statement may be clarified by examining Figure 15 and considering parallel light incident on the reflector. After passing through the front face, the light is divided into three sectors upon striking the three edges a, b, and c. Consider the single bundle of rays in the sector marked 1 determined by the real edges a and b. After the bundle hits this face it is reflected onto the other two faces marked 2 and 3, but also enclosed in the sector bounded by the reflections of a and b which are marked a' and b'. But edge c separates the single bundle from face 1 into two smaller bundles before reflecting the light out of the corner cube. Thus, the true equivalent diffracting aperture would be a circular aperture with six equally spaced wires of finite width emanating from the center of the circle. The diffraction pattern is different from that predicted by Eckhardt and results in a considerably larger pattern at large distances than that of the circular aperture as proposed by Eckhardt.

A picture of this pattern at a distance of 2.2 m from a 2.5 cm diameter corner cube reflector illuminated by a diverged laser beam is shown in Figure 16. The picture shows the pattern as elliptical but this is due to the offset camera angle. At a distance of 200 m the pattern from a 3.5 cm corner cube becomes a set of six spots located at the corners of a symmetric hexagon measuring 4 cm between opposite sides.

In order to estimate the diffraction spot size at large distances, each of the six sectors of light created by the 3.5 cm

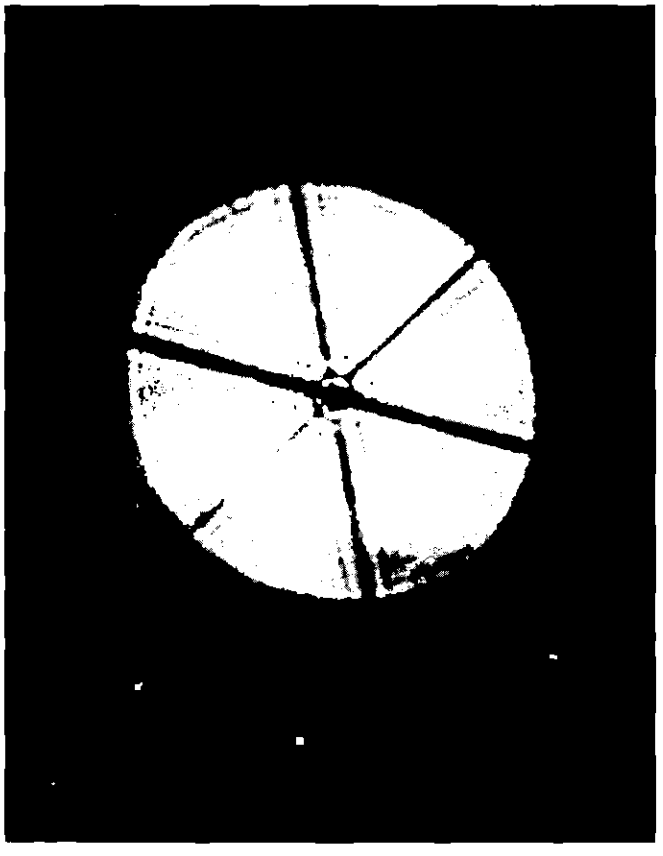

Figure 16. Diffraction Pattern of a Corner Cube Reflector at Short Range.

reflector is approximated as a circular bundle of rays 1.25 cm in diameter at the corner cube. The angular divergence through this equivalent aperture is given by the expression for diffraction by a circular aperture,[39]

$$\sin \theta \cong \theta = 2.44 \lambda/D$$

where θ is the total angular divergence, λ is the wavelength, and D is the aperture diameter. For D = 1.25 cm and λ = 500 nm, this gives $\theta = 0.975 \times 10^{-4}$ (radians) and the resulting spot size is the sum of the original diameter of 1.25 cm plus the increase of 34.5 cm for the diffraction effects at 3540 m. So the light returning to the receiver comes in six overlapping bundles approximately 36 cm in diameter each, with the centers of the bundles located at the corners of a hexagon 4 cm across.

BIBLIOGRAPHY

1. Air Quality Criteria for Nitrogen Oxides, Environmental Protection Agency, Air Pollution Control Office, Washington, D. C. (1971).

2. Homer J. Hall and William Bartok, Environmental Science and Technology, 5, 320-26 (1971).

3. R. D. Cadle, Journal of Colloid and Interface Science, 39, 25-31, (1972).

4. National Primary and Secondary Ambient Air Quality Standards, Environmental Protection Agency, Federal Register, Vol. 36, No. 84, Part II, 8185-8201 (1971).

5. Thomas R. Hauser and Carl M. Shy, Environmental Science and Technology, 6, 890-94 (1972).

6. J. H. Blacker and R. S. Brief, Chemosphere, 1, 43-46 (1972).

7. George P. Morgan, Guntis Ozolins, and Elbert C. Tabor, Science, 170, 289-96 (1970).

8. A. D. Snyder and G. W.Wooten, Monsanto Research Corporation, Dayton, Ohio, Final Report under National Air Pollution Control Administration Contract No. CPA-22-69-8 (1969).

9. M. E. Morrison and W. H. Corcoran, Analytical Chemistry, 39, 255-58 (1967).

10. F. Grum, D. Paine, and L. Zoeller, Applied Optics, 11, 93-8 (1972).

11. David T. Williams, Applied Optics, 11, 1658-9, (1972).

12. Helge Kildal and Robert L. Byer, Proceedings of the IEEE, 59, 1644- (1971).

13. Tomas Hirschfeld, S. Klainer, and R. Burton, Proceedings of the Technical Program Electro-Optical System Design Conference, 418-27 (1969).

14. A. E. Douglas and K. P. Huber, Canadian Journal of Physics, 43, 74-81 (1965).

15. G. Wilse Robinson, Maclyn McCarty, Jr., Mary C. Keelty, Journal of Chemical Physics, 28, 972-3 (1957).

16. J. K. Dixon, The Journal of Chemical Physics, 8, 157-60 (1940).

17. R. B. W. Pearse and A. G. Gaydon, The Identification of Molecular Spectra, Third Edition, John Wiley and Sons, Inc., New York (1963).

18. L. Burnelle, A. M. May, and R. A. Gangi, The Journal of Chemical Physics, 49, 561-9 (1968).

19. L. Burnelle, and K. P. Dressler, The Journal of Chemical Physics, 51, 2758-9 (1969).

20. William H. Fink, The Journal of Chemical Physics, 49, 5054-60 (1968).

21. K. Ya. Kondratyev, Radiation in the Atmosphere, Academic Press (1969).

22. P.W. Kruse, L. D. McGlauchlin, and R. B. McQuistan, Elements of Infrared Technology, John Wiley and Sons, Inc., New York (1963).

23. E. C. S. Megaw, Nature, 166, 1100-4 (1950).

24. Frank Gifford and A. H. Mikesell, Weather, 8, 195-7, (1953).

25. James P. Hansen and S. Madhu, Applied Optics, 11, 233-8 (1972).

26. M. P. Wohlers, Applied Optics, 11, 1389-98 (1972).

27. A. Consortini and L. Rochi, Applied Optics, 11, 1205-11, (1972).

28. William Braker and Allen L. Mossman, Matheson Gas Data Book, Fifth Edition, (1971).

29. John U. White, Journal of the Optical Society of America, 32, 285-8 (1942).

30. F. L. McNamara, Optical Engineering, 11, 9-12 (1972).

31. P. A. Leighton, Photochemistry of Air Pollution, Academic Press (1961).

32. C. B. Ludwig, R. Bartle, and M. Griggs, NASA CR-1380 (1969).

33. H. D. Eckhardt, Applied Optics, 10, 1559-66 (1971).

34. Frank H. Verhoek and Farrington Daniels, The Journal of the American Chemical Society, 53, 1250-63 (1931).

35. Leonard I. Shiff, Quantum Mechanics, Third Edition, McGraw-Hill Book Company (1968).

36. Dan Nurberger and A. B. F. Duncan, The Journal of Chemical Physics, 22, 1693-96 (1954).

37. S. Walker and H. Straw, Spectroscopy, Vol. 2, Chapman and Hall, Ltd., and Science Paperbacks (1962).

38. F. Reif, Fundamentals of Statistical and Thermal Physics, McGraw-Hill Book Company (1965).

39. F. A. Jenkins and H. E. White, Fundamentals of Optics, Third Edition, McGraw-Hill Book Co., Inc. (1957).